

Measurement of the Inclusive Electron Spectrum in Charmless Semileptonic B Decays Near the Kinematic Endpoint and Determination of $|V_{ub}|$

B. Aubert,¹ R. Barate,¹ D. Boutigny,¹ F. Couderc,¹ Y. Karyotakis,¹ J. P. Lees,¹ V. Poireau,¹ V. Tisserand,¹
A. Zghiche,¹ E. Grauges,² A. Palano,³ M. Pappagallo,³ A. Pompili,³ J. C. Chen,⁴ N. D. Qi,⁴ G. Rong,⁴
P. Wang,⁴ Y. S. Zhu,⁴ G. Eigen,⁵ I. Ofte,⁵ B. Stugu,⁵ G. S. Abrams,⁶ M. Battaglia,⁶ D. Best,⁶ A. B. Breon,⁶
D. N. Brown,⁶ J. Button-Shafer,⁶ R. N. Cahn,⁶ E. Charles,⁶ C. T. Day,⁶ M. S. Gill,⁶ A. V. Gritsan,⁶ Y. Groysman,⁶
R. G. Jacobsen,⁶ R. W. Kadel,⁶ J. Kadyk,⁶ L. T. Kerth,⁶ Yu. G. Kolomensky,⁶ G. Kukartsev,⁶ G. Lynch,⁶
L. M. Mir,⁶ P. J. Oddone,⁶ T. J. Orimoto,⁶ M. Pripstein,⁶ N. A. Roe,⁶ M. T. Ronan,⁶ W. A. Wenzel,⁶ M. Barrett,⁷
K. E. Ford,⁷ T. J. Harrison,⁷ A. J. Hart,⁷ C. M. Hawkes,⁷ S. E. Morgan,⁷ A. T. Watson,⁷ M. Fritsch,⁸ K. Goetzen,⁸
T. Held,⁸ H. Koch,⁸ B. Lewandowski,⁸ M. Pelizaeus,⁸ K. Peters,⁸ T. Schroeder,⁸ M. Steinke,⁸ J. T. Boyd,⁹
J. P. Burke,⁹ N. Chevalier,⁹ W. N. Cottingham,⁹ T. Cuhadar-Donszelmann,¹⁰ B. G. Fulsom,¹⁰ C. Hearty,¹⁰
N. S. Knecht,¹⁰ T. S. Mattison,¹⁰ J. A. McKenna,¹⁰ A. Khan,¹¹ P. Kyberd,¹¹ M. Saleem,¹¹ L. Teodorescu,¹¹
A. E. Blinov,¹² V. E. Blinov,¹² A. D. Bukin,¹² V. P. Druzhinin,¹² V. B. Golubev,¹² E. A. Kravchenko,¹²
A. P. Onuchin,¹² S. I. Serednyakov,¹² Yu. I. Skovpen,¹² E. P. Solodov,¹² A. N. Yushkov,¹² M. Bondioli,¹³
M. Bruinsma,¹³ M. Chao,¹³ S. Curry,¹³ I. Eschrich,¹³ D. Kirkby,¹³ A. J. Lankford,¹³ P. Lund,¹³ M. Mandelkern,¹³
R. K. Mommsen,¹³ W. Roethel,¹³ D. P. Stoker,¹³ C. Buchanan,¹⁴ B. L. Hartfiel,¹⁴ S. D. Foulkes,¹⁵ J. W. Gary,¹⁵
O. Long,¹⁵ B. C. Shen,¹⁵ K. Wang,¹⁵ L. Zhang,¹⁵ D. del Re,¹⁶ H. K. Hadavand,¹⁶ E. J. Hill,¹⁶ D. B. MacFarlane,¹⁶
H. P. Paar,¹⁶ S. Rahatlou,¹⁶ V. Sharma,¹⁶ J. W. Berryhill,¹⁷ C. Campagnari,¹⁷ A. Cunha,¹⁷ B. Dahmes,¹⁷
T. M. Hong,¹⁷ M. A. Mazur,¹⁷ J. D. Richman,¹⁷ W. Verkerke,¹⁷ T. W. Beck,¹⁸ A. M. Eisner,¹⁸ C. J. Flacco,¹⁸
C. A. Heusch,¹⁸ J. Kroseberg,¹⁸ W. S. Lockman,¹⁸ G. Nesom,¹⁸ T. Schalk,¹⁸ B. A. Schumm,¹⁸ A. Seiden,¹⁸
P. Spradlin,¹⁸ D. C. Williams,¹⁸ M. G. Wilson,¹⁸ J. Albert,¹⁹ E. Chen,¹⁹ G. P. Dubois-Felsmann,¹⁹ A. Dvoretzki,¹⁹
D. G. Hitlin,¹⁹ J. S. Minamora,¹⁹ I. Narsky,¹⁹ T. Piatenko,¹⁹ F. C. Porter,¹⁹ A. Ryd,¹⁹ A. Samuel,¹⁹
R. Andreassen,²⁰ G. Mancinelli,²⁰ B. T. Meadows,²⁰ M. D. Sokoloff,²⁰ F. Blanc,²¹ P. C. Bloom,²¹ S. Chen,²¹
W. T. Ford,²¹ J. F. Hirschauer,²¹ A. Kreisel,²¹ U. Nauenberg,²¹ A. Olivas,²¹ W. O. Ruddick,²¹ J. G. Smith,²¹
K. A. Ulmer,²¹ S. R. Wagner,²¹ J. Zhang,²¹ A. Chen,²² E. A. Eckhart,²² A. Soffer,²² W. H. Toki,²² R. J. Wilson,²²
Q. Zeng,²² D. Altenburg,²³ E. Feltresi,²³ A. Hauke,²³ B. Spaan,²³ T. Brandt,²⁴ J. Brose,²⁴ M. Dickopp,²⁴
V. Klose,²⁴ H. M. Lacker,²⁴ R. Nogowski,²⁴ S. Otto,²⁴ A. Petzold,²⁴ J. Schubert,²⁴ K. R. Schubert,²⁴ R. Schwierz,²⁴
J. E. Sundermann,²⁴ D. Bernard,²⁵ G. R. Bonneaud,²⁵ P. Grenier,²⁵ S. Schrenk,²⁵ Ch. Thiebaux,²⁵ G. Vasileiadis,²⁵
M. Verderi,²⁵ D. J. Bard,²⁶ P. J. Clark,²⁶ W. Gradl,²⁶ F. Muheim,²⁶ S. Playfer,²⁶ Y. Xie,²⁶ M. Andreotti,²⁷
D. Bettoni,²⁷ C. Bozzi,²⁷ R. Calabrese,²⁷ G. Cibinetto,²⁷ E. Luppi,²⁷ M. Negrini,²⁷ L. Piemontese,²⁷ F. Anulli,²⁸
R. Baldini-Feroli,²⁸ A. Calcaterra,²⁸ R. de Sangro,²⁸ G. Finocchiaro,²⁸ P. Patteri,²⁸ I. M. Peruzzi,²⁸ * M. Piccolo,²⁸
A. Zallo,²⁸ A. Buzzo,²⁹ R. Capra,²⁹ R. Contri,²⁹ M. Lo Vetere,²⁹ M. M. Macri,²⁹ M. R. Monge,²⁹ S. Passaggio,²⁹
C. Patrignani,²⁹ E. Robutti,²⁹ A. Santroni,²⁹ S. Tosi,²⁹ G. Brandenburg,³⁰ K. S. Chaisanguanthum,³⁰
M. Morii,³⁰ E. Won,³⁰ J. Wu,³⁰ R. S. Dubitzky,³¹ U. Langenegger,³¹ J. Marks,³¹ S. Schenk,³¹ U. Uwer,³¹
W. Bhimji,³² D. A. Bowerman,³² P. D. Dauncey,³² U. Egede,³² R. L. Flack,³² J. R. Gaillard,³² J. A. Nash,³²
M. B. Nikolich,³² W. Panduro Vazquez,³² X. Chai,³³ M. J. Charles,³³ W. F. Mader,³³ U. Mallik,³³ V. Ziegler,³³
J. Cochran,³⁴ H. B. Crawley,³⁴ V. Eyges,³⁴ W. T. Meyer,³⁴ S. Prell,³⁴ E. I. Rosenberg,³⁴ A. E. Rubin,³⁴
J. I. Yi,³⁴ G. Schott,³⁵ N. Arnaud,³⁶ M. Davier,³⁶ X. Giroux,³⁶ G. Grosdidier,³⁶ A. Höcker,³⁶ F. Le Diberder,³⁶
V. Lepeltier,³⁶ A. M. Lutz,³⁶ A. Oyangueren,³⁶ T. C. Petersen,³⁶ S. Plaszczynski,³⁶ S. Rodier,³⁶ P. Roudeau,³⁶
M. H. Schune,³⁶ A. Stocchi,³⁶ G. Wormser,³⁶ C. H. Cheng,³⁷ D. J. Lange,³⁷ M. C. Simani,³⁷ D. M. Wright,³⁷
A. J. Bevan,³⁸ C. A. Chavez,³⁸ I. J. Forster,³⁸ J. R. Fry,³⁸ E. Gabathuler,³⁸ R. Gamet,³⁸ K. A. George,³⁸
D. E. Hutchcroft,³⁸ R. J. Parry,³⁸ D. J. Payne,³⁸ K. C. Schofield,³⁸ C. Touramanis,³⁸ C. M. Cormack,³⁹
F. Di Lodovico,³⁹ W. Menges,³⁹ R. Sacco,³⁹ C. L. Brown,⁴⁰ G. Cowan,⁴⁰ H. U. Flaecher,⁴⁰ M. G. Green,⁴⁰
D. A. Hopkins,⁴⁰ P. S. Jackson,⁴⁰ T. R. McMahon,⁴⁰ S. Ricciardi,⁴⁰ F. Salvatore,⁴⁰ D. N. Brown,⁴¹ C. L. Davis,⁴¹

J. Allison,⁴² N. R. Barlow,⁴² R. J. Barlow,⁴² C. L. Edgar,⁴² M. C. Hodgkinson,⁴² M. P. Kelly,⁴² G. D. Lafferty,⁴² M. T. Naisbit,⁴² J. C. Williams,⁴² C. Chen,⁴³ W. D. Hulsbergen,⁴³ A. Jawahery,⁴³ D. Kovalskyi,⁴³ C. K. Lae,⁴³ D. A. Roberts,⁴³ G. Simi,⁴³ G. Blaylock,⁴⁴ C. Dallapiccola,⁴⁴ S. S. Hertzbach,⁴⁴ R. Kofler,⁴⁴ X. Li,⁴⁴ T. B. Moore,⁴⁴ S. Saremi,⁴⁴ H. Staengle,⁴⁴ S. Y. Willocq,⁴⁴ R. Cowan,⁴⁵ K. Koeneke,⁴⁵ G. Sciolla,⁴⁵ S. J. Sekula,⁴⁵ M. Spitznagel,⁴⁵ F. Taylor,⁴⁵ R. K. Yamamoto,⁴⁵ H. Kim,⁴⁶ P. M. Patel,⁴⁶ S. H. Robertson,⁴⁶ A. Lazzaro,⁴⁷ V. Lombardo,⁴⁷ F. Palombo,⁴⁷ J. M. Bauer,⁴⁸ L. Cremaldi,⁴⁸ V. Eschenburg,⁴⁸ R. Godang,⁴⁸ R. Kroeger,⁴⁸ J. Reidy,⁴⁸ D. A. Sanders,⁴⁸ D. J. Summers,⁴⁸ H. W. Zhao,⁴⁸ S. Brunet,⁴⁹ D. Côté,⁴⁹ P. Taras,⁴⁹ F. B. Viaud,⁴⁹ H. Nicholson,⁵⁰ N. Cavallo,^{51,†} G. De Nardo,⁵¹ F. Fabozzi,^{51,†} C. Gatto,⁵¹ L. Lista,⁵¹ D. Monorchio,⁵¹ P. Paolucci,⁵¹ D. Piccolo,⁵¹ C. Sciacca,⁵¹ M. Baak,⁵² H. Bulten,⁵² G. Raven,⁵² H. L. Snoek,⁵² L. Wilden,⁵² C. P. Jessop,⁵³ J. M. LoSecco,⁵³ T. Allmendinger,⁵⁴ G. Benelli,⁵⁴ K. K. Gan,⁵⁴ K. Honscheid,⁵⁴ D. Hufnagel,⁵⁴ P. D. Jackson,⁵⁴ H. Kagan,⁵⁴ R. Kass,⁵⁴ T. Pulliam,⁵⁴ A. M. Rahimi,⁵⁴ R. Ter-Antonyan,⁵⁴ Q. K. Wong,⁵⁴ N. L. Blount,⁵⁵ J. Brau,⁵⁵ R. Frey,⁵⁵ O. Igonkina,⁵⁵ M. Lu,⁵⁵ C. T. Potter,⁵⁵ R. Rahmat,⁵⁵ N. B. Sinev,⁵⁵ D. Strom,⁵⁵ J. Strube,⁵⁵ E. Torrence,⁵⁵ F. Galeazzi,⁵⁶ M. Margoni,⁵⁶ M. Morandin,⁵⁶ M. Posocco,⁵⁶ M. Rotondo,⁵⁶ F. Simonetto,⁵⁶ R. Stroili,⁵⁶ C. Voci,⁵⁶ M. Benayoun,⁵⁷ H. Briand,⁵⁷ J. Chauveau,⁵⁷ P. David,⁵⁷ L. Del Buono,⁵⁷ Ch. de la Vaissière,⁵⁷ O. Hamon,⁵⁷ M. J. J. John,⁵⁷ Ph. Leruste,⁵⁷ J. Malclès,⁵⁷ J. Ocariz,⁵⁷ L. Roos,⁵⁷ G. Therin,⁵⁷ P. K. Behera,⁵⁸ L. Gladney,⁵⁸ Q. H. Guo,⁵⁸ J. Panetta,⁵⁸ M. Biasini,⁵⁹ R. Covarelli,⁵⁹ S. Pacetti,⁵⁹ M. Pioppi,⁵⁹ C. Angelini,⁶⁰ G. Batignani,⁶⁰ S. Bettarini,⁶⁰ F. Bucci,⁶⁰ G. Calderini,⁶⁰ M. Carpinelli,⁶⁰ R. Cenci,⁶⁰ F. Forti,⁶⁰ M. A. Giorgi,⁶⁰ A. Lusiani,⁶⁰ G. Marchiori,⁶⁰ M. Morganti,⁶⁰ N. Neri,⁶⁰ E. Paoloni,⁶⁰ M. Rama,⁶⁰ G. Rizzo,⁶⁰ J. Walsh,⁶⁰ M. Haire,⁶¹ D. Judd,⁶¹ D. E. Wagoner,⁶¹ J. Biesiada,⁶² N. Danielson,⁶² P. Elmer,⁶² Y. P. Lau,⁶² C. Lu,⁶² J. Olsen,⁶² A. J. S. Smith,⁶² A. V. Telnov,⁶² F. Bellini,⁶³ G. Cavoto,⁶³ A. D’Orazio,⁶³ E. Di Marco,⁶³ R. Faccini,⁶³ F. Ferrarotto,⁶³ F. Ferroni,⁶³ M. Gaspero,⁶³ L. Li Gioi,⁶³ M. A. Mazzoni,⁶³ S. Morganti,⁶³ G. Piredda,⁶³ F. Polci,⁶³ F. Safai Tehrani,⁶³ C. Voena,⁶³ H. Schröder,⁶⁴ R. Waldi,⁶⁴ T. Adye,⁶⁵ N. De Groot,⁶⁵ B. Franek,⁶⁵ G. P. Gopal,⁶⁵ E. O. Olaiya,⁶⁵ F. F. Wilson,⁶⁵ R. Aleksan,⁶⁶ S. Emery,⁶⁶ A. Gaidot,⁶⁶ S. F. Ganzhur,⁶⁶ G. Graziani,⁶⁶ G. Hamel de Monchenault,⁶⁶ W. Kozanecki,⁶⁶ M. Legendre,⁶⁶ G. W. London,⁶⁶ B. Mayer,⁶⁶ G. Vasseur,⁶⁶ Ch. Yèche,⁶⁶ M. Zito,⁶⁶ M. V. Purohit,⁶⁷ A. W. Weidemann,⁶⁷ J. R. Wilson,⁶⁷ F. X. Yumiceva,⁶⁷ T. Abe,⁶⁸ M. T. Allen,⁶⁸ D. Aston,⁶⁸ R. Bartoldus,⁶⁸ N. Berger,⁶⁸ A. M. Boyarski,⁶⁸ O. L. Buchmueller,⁶⁸ R. Claus,⁶⁸ J. P. Coleman,⁶⁸ M. R. Convery,⁶⁸ M. Cristinziani,⁶⁸ J. C. Dingfelder,⁶⁸ D. Dong,⁶⁸ J. Dorfan,⁶⁸ D. Dujmic,⁶⁸ W. Dunwoodie,⁶⁸ S. Fan,⁶⁸ R. C. Field,⁶⁸ T. Glanzman,⁶⁸ S. J. Gowdy,⁶⁸ T. Hadig,⁶⁸ V. Halyo,⁶⁸ C. Hast,⁶⁸ T. Hryn’ova,⁶⁸ W. R. Innes,⁶⁸ M. H. Kelsey,⁶⁸ P. Kim,⁶⁸ M. L. Kocian,⁶⁸ D. W. G. S. Leith,⁶⁸ J. Libby,⁶⁸ S. Luitz,⁶⁸ V. Luth,⁶⁸ H. L. Lynch,⁶⁸ H. Marsiske,⁶⁸ R. Messner,⁶⁸ D. R. Muller,⁶⁸ C. P. O’Grady,⁶⁸ V. E. Ozcan,⁶⁸ A. Perazzo,⁶⁸ M. Perl,⁶⁸ B. N. Ratcliff,⁶⁸ A. Roodman,⁶⁸ A. A. Salnikov,⁶⁸ R. H. Schindler,⁶⁸ J. Schwiening,⁶⁸ A. Snyder,⁶⁸ J. Stelzer,⁶⁸ D. Su,⁶⁸ M. K. Sullivan,⁶⁸ K. Suzuki,⁶⁸ S. K. Swain,⁶⁸ J. M. Thompson,⁶⁸ J. Va’vra,⁶⁸ N. van Bakel,⁶⁸ M. Weaver,⁶⁸ A. J. R. Weinstein,⁶⁸ W. J. Wisniewski,⁶⁸ M. Wittgen,⁶⁸ D. H. Wright,⁶⁸ A. K. Yarritu,⁶⁸ K. Yi,⁶⁸ C. C. Young,⁶⁸ P. R. Burchat,⁶⁹ A. J. Edwards,⁶⁹ S. A. Majewski,⁶⁹ B. A. Petersen,⁶⁹ C. Roat,⁶⁹ M. Ahmed,⁷⁰ S. Ahmed,⁷⁰ M. S. Alam,⁷⁰ R. Bula,⁷⁰ J. A. Ernst,⁷⁰ M. A. Saeed,⁷⁰ F. R. Wappler,⁷⁰ S. B. Zain,⁷⁰ W. Bugg,⁷¹ M. Krishnamurthy,⁷¹ S. M. Spanier,⁷¹ R. Eckmann,⁷² J. L. Ritchie,⁷² A. Satpathy,⁷² R. F. Schwitters,⁷² J. M. Izen,⁷³ I. Kitayama,⁷³ X. C. Lou,⁷³ S. Ye,⁷³ F. Bianchi,⁷⁴ M. Bona,⁷⁴ F. Gallo,⁷⁴ D. Gamba,⁷⁴ M. Bomben,⁷⁵ L. Bosisio,⁷⁵ C. Cartaro,⁷⁵ F. Cossutti,⁷⁵ G. Della Ricca,⁷⁵ S. Dittongo,⁷⁵ S. Grancagnolo,⁷⁵ L. Lanceri,⁷⁵ L. Vitale,⁷⁵ V. Azzolini,⁷⁶ F. Martinez-Vidal,⁷⁶ R. S. Panvini,^{77,‡} Sw. Banerjee,⁷⁸ B. Bhuyan,⁷⁸ C. M. Brown,⁷⁸ D. Fortin,⁷⁸ K. Hamano,⁷⁸ R. Kowalewski,⁷⁸ J. M. Roney,⁷⁸ R. J. Sobie,⁷⁸ J. J. Back,⁷⁹ P. F. Harrison,⁷⁹ T. E. Latham,⁷⁹ G. B. Mohanty,⁷⁹ H. R. Band,⁸⁰ X. Chen,⁸⁰ B. Cheng,⁸⁰ S. Dasu,⁸⁰ M. Datta,⁸⁰ A. M. Eichenbaum,⁸⁰ K. T. Flood,⁸⁰ M. T. Graham,⁸⁰ J. J. Hollar,⁸⁰ J. R. Johnson,⁸⁰ P. E. Kutter,⁸⁰ H. Li,⁸⁰ R. Liu,⁸⁰ B. Mellado,⁸⁰ A. Mihalysi,⁸⁰ A. K. Mohapatra,⁸⁰ Y. Pan,⁸⁰ M. Pierini,⁸⁰ R. Prepost,⁸⁰ P. Tan,⁸⁰ S. L. Wu,⁸⁰ Z. Yu,⁸⁰ and H. Neal⁸¹

(The BABAR Collaboration)

¹Laboratoire de Physique des Particules, F-74941 Annecy-le-Vieux, France

²IFAE, Universitat Autònoma de Barcelona, E-08193 Bellaterra, Barcelona, Spain

³Università di Bari, Dipartimento di Fisica and INFN, I-70126 Bari, Italy

⁴Institute of High Energy Physics, Beijing 100039, China

⁵University of Bergen, Institute of Physics, N-5007 Bergen, Norway

⁶Lawrence Berkeley National Laboratory and University of California, Berkeley, California 94720, USA

⁷University of Birmingham, Birmingham, B15 2TT, United Kingdom

⁸Ruhr Universität Bochum, Institut für Experimentalphysik 1, D-44780 Bochum, Germany

⁹University of Bristol, Bristol BS8 1TL, United Kingdom

¹⁰University of British Columbia, Vancouver, British Columbia, Canada V6T 1Z1

- ¹¹ Brunel University, Uxbridge, Middlesex UB8 3PH, United Kingdom
¹² Budker Institute of Nuclear Physics, Novosibirsk 630090, Russia
¹³ University of California at Irvine, Irvine, California 92697, USA
¹⁴ University of California at Los Angeles, Los Angeles, California 90024, USA
¹⁵ University of California at Riverside, Riverside, California 92521, USA
¹⁶ University of California at San Diego, La Jolla, California 92093, USA
¹⁷ University of California at Santa Barbara, Santa Barbara, California 93106, USA
¹⁸ University of California at Santa Cruz, Institute for Particle Physics, Santa Cruz, California 95064, USA
¹⁹ California Institute of Technology, Pasadena, California 91125, USA
²⁰ University of Cincinnati, Cincinnati, Ohio 45221, USA
²¹ University of Colorado, Boulder, Colorado 80309, USA
²² Colorado State University, Fort Collins, Colorado 80523, USA
²³ Universität Dortmund, Institut für Physik, D-44221 Dortmund, Germany
²⁴ Technische Universität Dresden, Institut für Kern- und Teilchenphysik, D-01062 Dresden, Germany
²⁵ Ecole Polytechnique, LLR, F-91128 Palaiseau, France
²⁶ University of Edinburgh, Edinburgh EH9 3JZ, United Kingdom
²⁷ Università di Ferrara, Dipartimento di Fisica and INFN, I-44100 Ferrara, Italy
²⁸ Laboratori Nazionali di Frascati dell'INFN, I-00044 Frascati, Italy
²⁹ Università di Genova, Dipartimento di Fisica and INFN, I-16146 Genova, Italy
³⁰ Harvard University, Cambridge, Massachusetts 02138, USA
³¹ Universität Heidelberg, Physikalisches Institut, Philosophenweg 12, D-69120 Heidelberg, Germany
³² Imperial College London, London, SW7 2AZ, United Kingdom
³³ University of Iowa, Iowa City, Iowa 52242, USA
³⁴ Iowa State University, Ames, Iowa 50011-3160, USA
³⁵ Universität Karlsruhe, Institut für Experimentelle Kernphysik, D-76021 Karlsruhe, Germany
³⁶ Laboratoire de l'Accélérateur Linéaire, F-91898 Orsay, France
³⁷ Lawrence Livermore National Laboratory, Livermore, California 94550, USA
³⁸ University of Liverpool, Liverpool L69 7ZE, United Kingdom
³⁹ Queen Mary, University of London, E1 4NS, United Kingdom
⁴⁰ University of London, Royal Holloway and Bedford New College, Egham, Surrey TW20 0EX, United Kingdom
⁴¹ University of Louisville, Louisville, Kentucky 40292, USA
⁴² University of Manchester, Manchester M13 9PL, United Kingdom
⁴³ University of Maryland, College Park, Maryland 20742, USA
⁴⁴ University of Massachusetts, Amherst, Massachusetts 01003, USA
⁴⁵ Massachusetts Institute of Technology, Laboratory for Nuclear Science, Cambridge, Massachusetts 02139, USA
⁴⁶ McGill University, Montréal, Québec, Canada H3A 2T8
⁴⁷ Università di Milano, Dipartimento di Fisica and INFN, I-20133 Milano, Italy
⁴⁸ University of Mississippi, University, Mississippi 38677, USA
⁴⁹ Université de Montréal, Physique des Particules, Montréal, Québec, Canada H3C 3J7
⁵⁰ Mount Holyoke College, South Hadley, Massachusetts 01075, USA
⁵¹ Università di Napoli Federico II, Dipartimento di Scienze Fisiche and INFN, I-80126, Napoli, Italy
⁵² NIKHEF, National Institute for Nuclear Physics and High Energy Physics, NL-1009 DB Amsterdam, The Netherlands
⁵³ University of Notre Dame, Notre Dame, Indiana 46556, USA
⁵⁴ Ohio State University, Columbus, Ohio 43210, USA
⁵⁵ University of Oregon, Eugene, Oregon 97403, USA
⁵⁶ Università di Padova, Dipartimento di Fisica and INFN, I-35131 Padova, Italy
⁵⁷ Universités Paris VI et VII, Laboratoire de Physique Nucléaire et de Hautes Energies, F-75252 Paris, France
⁵⁸ University of Pennsylvania, Philadelphia, Pennsylvania 19104, USA
⁵⁹ Università di Perugia, Dipartimento di Fisica and INFN, I-06100 Perugia, Italy
⁶⁰ Università di Pisa, Dipartimento di Fisica, Scuola Normale Superiore and INFN, I-56127 Pisa, Italy
⁶¹ Prairie View A&M University, Prairie View, Texas 77446, USA
⁶² Princeton University, Princeton, New Jersey 08544, USA
⁶³ Università di Roma La Sapienza, Dipartimento di Fisica and INFN, I-00185 Roma, Italy
⁶⁴ Universität Rostock, D-18051 Rostock, Germany
⁶⁵ Rutherford Appleton Laboratory, Chilton, Didcot, Oxon, OX11 0QX, United Kingdom
⁶⁶ DSM/Dapnia, CEA/Saclay, F-91191 Gif-sur-Yvette, France
⁶⁷ University of South Carolina, Columbia, South Carolina 29208, USA
⁶⁸ Stanford Linear Accelerator Center, Stanford, California 94309, USA
⁶⁹ Stanford University, Stanford, California 94305-4060, USA
⁷⁰ State University of New York, Albany, New York 12222, USA
⁷¹ University of Tennessee, Knoxville, Tennessee 37996, USA
⁷² University of Texas at Austin, Austin, Texas 78712, USA
⁷³ University of Texas at Dallas, Richardson, Texas 75083, USA
⁷⁴ Università di Torino, Dipartimento di Fisica Sperimentale and INFN, I-10125 Torino, Italy

⁷⁵Università di Trieste, Dipartimento di Fisica and INFN, I-34127 Trieste, Italy

⁷⁶IFIC, Universitat de Valencia-CSIC, E-46071 Valencia, Spain

⁷⁷Vanderbilt University, Nashville, Tennessee 37235, USA

⁷⁸University of Victoria, Victoria, British Columbia, Canada V8W 3P6

⁷⁹Department of Physics, University of Warwick, Coventry CV4 7AL, United Kingdom

⁸⁰University of Wisconsin, Madison, Wisconsin 53706, USA

⁸¹Yale University, New Haven, Connecticut 06511, USA

We present a measurement of the inclusive electron spectrum in $B \rightarrow X_u e \nu$ decays near the kinematic limit for $B \rightarrow X_c e \nu$ transitions, using a sample of 88 million $B\bar{B}$ pairs recorded by the BABAR detector at the $\Upsilon(4S)$ resonance. Partial branching fraction measurements are performed in five overlapping intervals of the electron momentum; for the interval of 2.0–2.6 GeV/c we obtain $\Delta\mathcal{B}(B \rightarrow X_u e \nu) = (0.572 \pm 0.041_{stat} \pm 0.065_{syst}) \times 10^{-3}$. Combining this result with shape function parameters extracted from BABAR measurements of moments of the inclusive photon spectrum in $B \rightarrow X_s \gamma$ decays and moments of the hadron mass and lepton energy spectra in $B \rightarrow X_c \ell \nu$ decays we determine $|V_{ub}| = (4.44 \pm 0.25_{exp} \pm 0.42_{SF} \pm 0.38_{theory}) \times 10^{-3}$. Here the first error represents the combined statistical and systematic experimental uncertainties of the partial branching fraction measurement, the second error refers to the uncertainty of the determination of the shape function parameters, and the third error is due to theoretical uncertainties in the QCD calculations.

PACS numbers: 13.20.He, 12.15.Hh, 12.38.Qk, 14.40.Nd

I. INTRODUCTION

The Cabibbo-Kobayashi-Maskawa (CKM) matrix element V_{ub} , the coupling of the b quark to the u quark, is a fundamental parameter of the Standard Model. It is one of the smallest and least known elements of the CKM matrix. With the increasingly precise measurements of decay-time-dependent CP asymmetries in B -meson decays, in particular the angle β [1, 2], improved measurements of the magnitude of V_{ub} will allow for stringent experimental tests of the Standard Model mechanism for CP violation [3]. This is best illustrated in terms of the unitarity triangle, the graphical representation of the unitarity condition for the CKM matrix, for which the length of the side that is opposite to the angle β is proportional to $|V_{ub}|$.

The extraction of $|V_{ub}|$ is a challenge, both theoretically and experimentally. Experimentally, the principal challenge is to separate the signal $B \rightarrow X_u e \nu$ decays from the 50 times larger $B \rightarrow X_c e \nu$ background. This can be achieved by selecting regions of phase space in which this background is highly suppressed. In the rest frame of the B meson, the kinematic endpoint of the electron spectrum is ~ 2.3 GeV/c for the dominant $B \rightarrow X_c e \nu$ decays and ~ 2.6 GeV/c for $B \rightarrow X_u e \nu$ decays. Thus the spectrum above 2.3 GeV/c is dominated by electrons from $B \rightarrow X_u e \nu$ transitions. This allows for a relatively precise measurement, largely free from $B\bar{B}$ background, in a 300 MeV/c interval that covers approximately 10% of the total electron spectrum for charmless semileptonic B decays. In the $\Upsilon(4S)$ rest frame, the finite momenta of

the B mesons cause additional spread of the electron momenta of ~ 200 MeV/c, extending the endpoints to higher momenta.

The weak decay rate for $b \rightarrow ue\nu$ can be calculated at the parton level. It is proportional to $|V_{ub}|^2$ and m_b^5 , where m_b refers to the b -quark mass. To relate the semileptonic decay rate of the B meson to $|V_{ub}|$, the parton-level calculations have to be corrected for perturbative and non-perturbative QCD effects. These corrections can be calculated using various techniques: heavy quark expansions (HQE) [4] and QCD factorization [5]. Both approaches separate perturbative from non-perturbative expressions and sort terms in powers of $1/m_b$. HQE is appropriate for the calculations of total inclusive B decay rates and for partial B decay rates integrated over sufficiently large regions of phase space where the mass and momentum of the final state hadron are large compared to Λ_{QCD} . QCD factorization is better suited for calculations of partial rates and spectra near the kinematic boundaries where the hadronic mass is small. In this region the spectra are affected by the distribution of the b -quark momentum inside the B meson [5], which can be described by a structure or shape function (SF), in addition to weak annihilation and other non-perturbative effects. Extrapolation from the limited momentum range near the endpoint to the full spectrum is a difficult task, because the SF cannot be calculated. To leading order, the SF should be universal for all $b \rightarrow q$ transitions (here q represents a light quark) [6, 7]. Several functional forms for the SF, which generally depend on two parameters related to the mass and kinetic energy of the b -quark, $\bar{\Lambda}$ or m_b , and λ_1 or μ_π^2 , have been proposed. The values and precise definitions of these parameters depend on the specific ansatz for the SF, the mass renormalization scheme, and the renormalization scale chosen.

In this paper, we present a measurement of the inclusive electron momentum spectrum in charmless semilep-

*Also with Università di Perugia, Dipartimento di Fisica, Perugia, Italy

[†]Also with Università della Basilicata, Potenza, Italy

[‡]Deceased

tonic B decays, averaged over charged and neutral B mesons, near the kinematic endpoint. We report measurements of the partial branching fractions in five overlapping momentum intervals. The upper limit is fixed at 2.6 GeV/ c , while the lower limit varies from 2.0 GeV/ c to 2.4 GeV/ c . By extending the interval for the signal extraction down to 2.0 GeV/ c , we capture about 25% of the total signal electron spectrum, but also much larger $B \rightarrow X_c e \nu$ backgrounds. Inclusive measurements of $|V_{ub}|$ have been performed by several experiments operating at the $\Upsilon(4S)$ resonance, namely ARGUS [8], CLEO [9, 10], BABAR [11], and recently Belle [12], and experiments operating at the Z^0 resonance, namely L3 [13], ALEPH [14], DELPHI [15], and OPAL [16]. This analysis is based on a method similar to the one used in previous measurements of the lepton spectrum near the kinematic endpoint [8, 9]. The results presented here supersede those of the preliminary analysis reported by the BABAR Collaboration [11].

The extraction of $|V_{ub}|$ relies on two different theoretical calculations of the differential decay rates for $B \rightarrow X_u e \nu$ and $B \rightarrow X_s \gamma$: the original work by DeFazio and Neubert (DN) [17], and Kagan and Neubert [18], and the more comprehensive recent calculations by Bosch, Lange, Neubert, and Paz (BLNP) [19–24].

The DN calculations allow for the extrapolation of the observed partial $B \rightarrow X_u e \nu$ decay rate above a certain electron momentum to the total inclusive $B \rightarrow X_u e \nu$ decay rate using the measured SF parameters and a subsequent translation of the total decay rate to $|V_{ub}|$. The theoretical uncertainties on the rate predictions are estimated to be of order 10–20%.

The BLNP authors have presented a systematic treatment of the SF effects, incorporated all known corrections to the differential decay rates, and provided an interpolation between the HQE and the SF regions. They have also performed a detailed analysis of the theoretical uncertainties. The calculations directly relate the partial decay rate to $|V_{ub}|$. While the calculations by BLNP are to supersede the earlier work by DN, we use both approaches to allow for a direct comparison of the two calculations, and also a comparison with previous measurements based on the DN calculations. We adopt the SF parameters extracted by the BABAR Collaboration: for the DN method we rely on the photon spectrum in $B \rightarrow X_s \gamma$ decays [25]; for the more recent BLNP method, we also use SF parameters derived from the photon spectrum, its moments, the hadron-mass and lepton-energy moments in inclusive $B \rightarrow X_c \ell \nu$ decays [26], and the combination of all moments measured by the BABAR Collaboration [27].

II. DATA SAMPLE, DETECTOR, AND SIMULATION

The data used in this analysis were recorded with the BABAR detector at the PEP-II energy-asymmetric e^+e^- collider. The data sample of 88 million $B\bar{B}$ events, cor-

responding to an integrated luminosity of 80.4 fb $^{-1}$, was collected at the $\Upsilon(4S)$ resonance. An additional sample of 9.5 fb $^{-1}$ was recorded at a center-of-mass (c.m.) energy 40 MeV below the $\Upsilon(4S)$ resonance, *i.e.* just below the threshold for $B\bar{B}$ production. This off-resonance data sample is used to subtract the non- $B\bar{B}$ contributions from the data collected on the $\Upsilon(4S)$ resonance. The relative normalization of the two data samples has been derived from luminosity measurements, which are based on the number of detected $\mu^+\mu^-$ pairs and the QED cross section for $e^+e^- \rightarrow \mu^+\mu^-$ production, adjusted for the small difference in center-of-mass energy.

The BABAR detector has been described in detail elsewhere [28]. The most important components for this study are the charged-particle tracking system, consisting of a five-layer silicon detector and a 40-layer drift chamber, and the electromagnetic calorimeter assembled from 6580 CsI(Tl) crystals. These detector components operate in a 1.5-T solenoidal magnetic field. Electron candidates are selected on the basis of the ratio of the energy detected in the calorimeter to the track momentum, the calorimeter shower shape, the energy loss in the drift chamber, and the angle of the photons reconstructed in a ring-imaging Cherenkov detector.

The electron identification efficiency and the probabilities to misidentify a pion, kaon, or proton as an electron have been measured [29] as a function of the laboratory momentum and angles with clean samples of tracks selected from data. Within the acceptance of the calorimeter, defined by the polar angle in the laboratory frame, $-0.72 < \cos\theta_{lab} < 0.92$, the average electron identification efficiency is 92%. The average hadron misidentification rate is about 0.1%.

We use Monte Carlo (MC) techniques to simulate the production and decay of B mesons, and the detector response [30], to estimate signal and background efficiencies, and to extract the observed signal and background distributions. The simulated sample of generic $B\bar{B}$ events exceeds the $B\bar{B}$ data sample by about a factor of three.

Information from studies of selected control data samples on efficiencies and resolutions is used to improve the accuracy of the simulation. Comparisons of data with the MC simulations have revealed small differences in the tracking efficiencies, which have been corrected for. No significant impact of non-Gaussian resolution tails has been found for high momentum tracks in the endpoint region. The MC simulations include radiative effects such as bremsstrahlung in the detector material and QED initial and final state radiation [31]. Adjustments for small variations of the beam energy over time have also been included.

In the MC simulations the branching fractions for hadronic B and D decays are based on values reported in the Review of Particle Physics [32]. The simulation of charmless semileptonic decays, $B \rightarrow X_u e \nu$, is based on a heavy quark expansion to $\mathcal{O}(\alpha_s)$ [17]. This calculation produces a continuous spectrum of hadronic states.

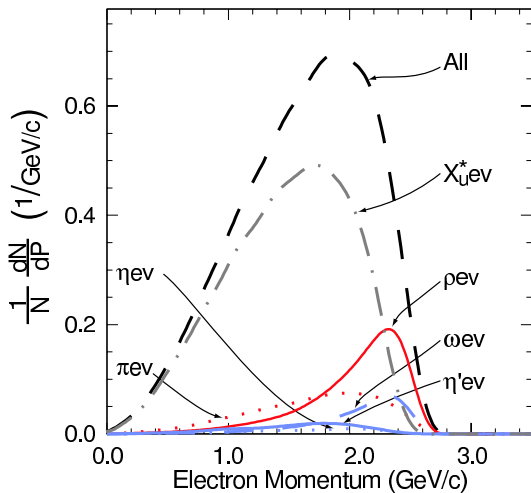


FIG. 1: MC-generated electron momentum spectra for various charmless semileptonic B decays: $B \rightarrow \pi e \nu$, $B \rightarrow \rho e \nu$, $B \rightarrow \omega e \nu$, $B \rightarrow \eta e \nu$, $B \rightarrow \eta' e \nu$, the sum of B -meson decay modes to non-resonant and higher-mass resonance states ($X_u^* e \nu$), and the sum of all decay modes (All). The spectra are normalized to a total rate of 1.0.

The hadronization of X_u with masses above $2m_\pi$ is performed by JETSET [33]. The motion of the b quark inside the B meson is implemented with the SF parameterization given in [17]. Three-body decays to low-mass hadrons, ($X_u = \pi, \rho, \omega, \eta, \eta'$), are simulated separately using the ISGW2 model [34] and mixed with decays to non-resonant and higher mass resonant states X_u^* , so that the cumulative distributions of the hadron mass, the momentum transfer squared, and the electron momentum reproduce the HQE calculation as closely as possible. The generated electron spectrum is reweighted to accommodate variations due to specific choices of the SF parameters.

The MC-generated electron-momentum distributions for $B \rightarrow X_u e \nu$ decays are shown in Fig. 1, for individual decay modes and for their sum. Here and throughout the paper, the electron momentum and all other kinematic variables are measured in the $\Upsilon(4S)$ rest frame, unless stated otherwise. Above $2 \text{ GeV}/c$, the principal signal contributions are from decays involving the light mesons π, ρ , and ω , and also some higher mass resonant and non-resonant states X_u^* .

For the simulation of the dominant $B \rightarrow X_c e \nu$ decays, we have chosen a variety of models. For $B \rightarrow D e \nu$ and $B \rightarrow D^* e \nu$ decays we use parameterizations [35–37] of the form factors, based on heavy quark effective theory (HQET). Decays to pseudoscalar mesons are described by a single form factor $F_D(w)/F_D(1) = 1 - \rho_D^2(w-1)$, where the variable w is the scalar product of the B and D meson four-vector velocities and is equal to the relativistic boost of the D meson in the B meson rest frame. The linear slope ρ_D^2 has been measured by the CLEO [38] and Belle [39] Collaborations. We use the average value, $\rho_D^2 =$

0.72 ± 0.12 . The differential decay rate for $B \rightarrow D^* e \nu$ can be described by three amplitudes, which depend on three parameters: ρ^2 , R_1 , and R_2 . We adopt values recently measured by BABAR [40]: $\rho^2 = 0.769 \pm 0.043 \pm 0.032$, $R_1 = 1.328 \pm 0.060 \pm 0.025$, and $R_2 = 0.920 \pm 0.048 \pm 0.013$. Here the parameter ρ^2 is the slope assuming a linear dependence of the form factor on the variable w . The quoted errors reflect the statistical and systematic uncertainties.

We use the ISGW2 [34] model for various decays to higher-mass D^{**} resonances. We have adopted a prescription by Goity and Roberts [41] for the non-resonant $B \rightarrow D^{(*)} \pi e \nu$ decays.

The shapes of the MC-generated electron spectra for individual $B \rightarrow X_c e \nu$ decays are shown in Fig. 2. Above $2 \text{ GeV}/c$ the principal background contributions are from decays involving the lower-mass charm mesons, D^* and D . Higher-mass and non-resonant charm states are expected to contribute at lower electron momenta. The relative contributions of the individual $B \rightarrow X_c e \nu$ decay modes are adjusted to match the data by a fit to the observed spectrum (see below).

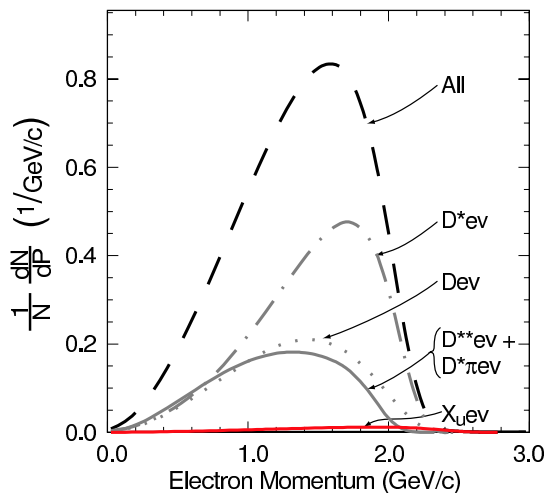


FIG. 2: MC-generated electron momentum spectra for various $B \rightarrow X_c e \nu$ decay modes: $B \rightarrow D e \nu$, $B \rightarrow D^* e \nu$, $B \rightarrow D^{**} e \nu$, $B \rightarrow D^{(*)} \pi e \nu$, and $B \rightarrow X_u e \nu$, and the sum of all decay modes (All). The signal $B \rightarrow X_u e \nu$ spectrum is shown for comparison. The spectra are normalized to a total rate of 1.0.

III. ANALYSIS

A. Event Selection

We select events with a semileptonic B decay by requiring an electron with momentum $p_e > 1.1 \text{ GeV}/c$. To reject electrons from the decay $J/\psi \rightarrow e^+ e^-$, we combine the electron candidate with any second electron of

opposite charge and reject the combination, if the invariant mass of the pair falls in the interval $3.00 < m_{ee} < 3.15 \text{ GeV}/c^2$.

To suppress background from non- $B\bar{B}$ events, primarily low-multiplicity QED (including $\tau^+\tau^-$ pairs) and $e^+e^- \rightarrow q\bar{q}$ processes (here q represents any of the u, d, s or c quarks), we veto events with fewer than four charged tracks. We also require that the ratio of the second to the zeroth Fox-Wolfram moment [42], \mathcal{R}_2 , not exceed 0.5. \mathcal{R}_2 is calculated including all detected charged particles and photons. For events with an electron in the momentum interval of 2.0 to 2.6 GeV/c , these two criteria reduce the non- $B\bar{B}$ background by a factor of about 6, while retaining more than 80% of the signal events.

In semileptonic B decays, the neutrino carries sizable energy. In events in which the only undetected particle is this neutrino, the neutrino four-momentum can be inferred from the missing momentum, $p_{miss} = (E_{miss}, \vec{p}_{miss})$, the difference between the four-momentum of the two colliding-beam particles, and the sum of the four-momenta of all detected particles, charged and neutral. To improve the reconstruction of the missing momentum, we impose a number of requirements on the charged and neutral particles. Charged tracks are required to have a minimum transverse momentum of 0.2 GeV/c and a maximum momentum of 10 GeV/c in the laboratory frame. Charged tracks are also restricted in polar angle to $-0.82 < \cos\theta_{lab} < 0.92$ and they are required to originate close to the beam-beam interaction point. The individual photon energy in the laboratory frame is required to exceed 30 MeV. The selection of semileptonic B decays is enhanced by requiring $|\vec{p}_{miss}| > 0.5 \text{ GeV}/c$, and that \vec{p}_{miss} points into the detector fiducial volume, $|\cos\theta_{miss}| < 0.9$, thereby effectively reducing the impact of particle losses close to the beams. Furthermore, since in semileptonic B decays with a high-momentum electron, the neutrino and the electron are emitted preferentially in opposite directions, we require that the angle $\Delta\alpha$ between these two particles fulfill the condition $\cos\Delta\alpha < 0.4$. These requirements for the missing momentum reduce the continuum background from QED processes and $e^+e^- \rightarrow q\bar{q}$ production by an additional factor of 3, while the signal loss is less than 20%.

The stated selection criteria result in an efficiency (including effects of bremsstrahlung) of 35 – 50% for selecting $B \rightarrow X_u e \nu$ decays; its dependence on the electron momentum is shown in Fig. 3.

B. Background Subtraction

The spectrum of the highest momentum electron in events selected by the criteria described above is shown in Fig. 4a, separately for data recorded on and below the $\Upsilon(4S)$ resonance. The data collected on the $\Upsilon(4S)$ resonance include contributions from $B\bar{B}$ events and non- $B\bar{B}$ background. The latter is measured using off-resonance

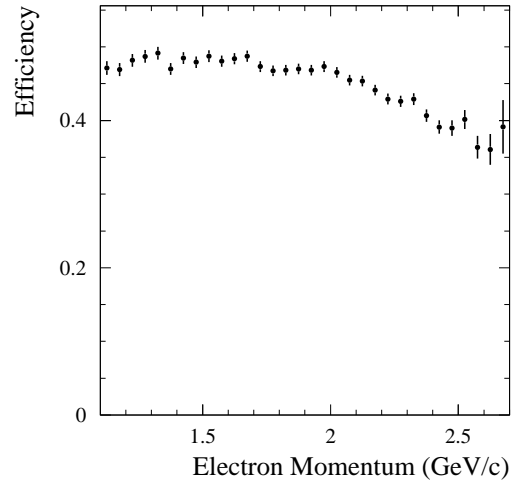


FIG. 3: Selection efficiency for events with $B \rightarrow X_u e \nu$ decays as a function of the electron momentum. The error bars represent the statistical errors.

data, collected below $B\bar{B}$ production threshold, and using on-resonance data above 2.8 GeV/c , *i.e.*, above the endpoint for electrons from B decays. The $B\bar{B}$ background to the $B \rightarrow X_u e \nu$ spectrum is estimated from MC simulation, with the normalization of the individual contributions determined by a fit to the total observed spectrum.

1. Non- $B\bar{B}$ Background

To determine the non- $B\bar{B}$ background we perform a χ^2 fit to the off-resonance data in the momentum interval of 1.1 to 3.5 GeV/c and to on-resonance data in the momentum interval of 2.8 to 3.5 GeV/c . Since the c.m. energy for the off-resonance data is 0.4% lower than for the on-resonance data, we scale the electron momenta for the off-resonance data by the ratio of the c.m. energies.

The relative normalization for the two data sets is

$$r_L = \frac{s_{OFF}}{s_{ON}} \frac{\int L_{ON} dt}{\int L_{OFF} dt} = 8.433 \pm 0.004 \pm 0.021,$$

where s and $\int L dt$ refer to the c.m. energy squared and integrated luminosity of the two data sets. The statistical uncertainty of r_L is determined by the number of detected $\mu^+\mu^-$ pairs used for the measurement of the integrated luminosity; the systematic error of the ratio is estimated to be 0.25%.

The χ^2 for the fit to the non- $B\bar{B}$ events is defined as follows,

$$\chi_c^2 = \sum_i \frac{(f(\vec{a}, p_i) - r_L n_i)^2}{r_L^2 n_i} + \sum_j \frac{(f(\vec{a}, p_j) - N_j)^2}{N_j}. \quad (1)$$

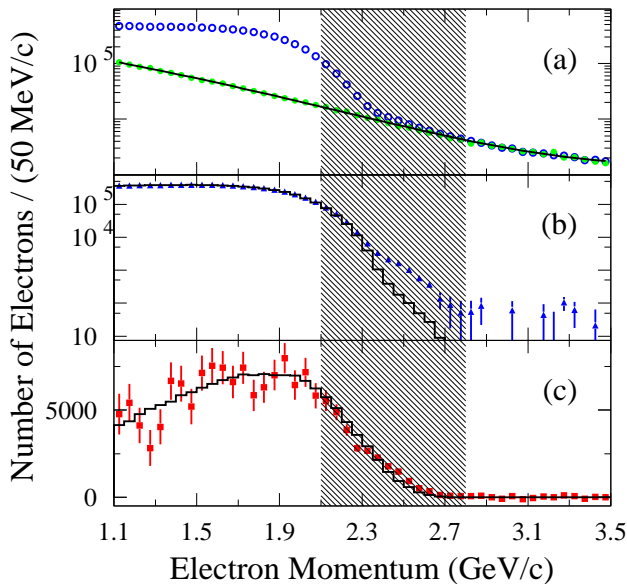


FIG. 4: (color online) Electron momentum spectra in the $\Upsilon(4S)$ rest frame: (a) on-resonance data (open circles – blue), scaled off-resonance data (solid circles – green); the solid line shows the result of the fit to the non- $B\bar{B}$ events using both on- and off-resonance data; (b) on-resonance data after subtraction of the fitted non- $B\bar{B}$ background (triangles – blue) compared to simulated $B\bar{B}$ background that is adjusted by the combined fit to the on- and off-resonance data (histogram); (c) on-resonance data after subtraction of all backgrounds (linear vertical scale, data points – red), compared to the simulated $B \rightarrow X_u e \nu$ signal spectrum (histogram); the error bars indicate errors from the fit, which include the uncertainties in the fitted scale factors for non- $B\bar{B}$ and $X_c e \nu$ backgrounds. The shaded area indicates the momentum interval for which the on-resonance data are combined into a single bin for the purpose of reducing the sensitivity of the fit to the shape of the signal spectrum in this region.

Here n_i and N_j refer to the number of selected events in the off- and on-resonance samples, for the i -th or j -th momentum bin ($p_j > 2.8$ GeV/ c), and \vec{a} is the set of free parameters of the fit. For the function approximating the momentum spectrum, we have chosen an exponential expression of the form

$$f(\vec{a}, p) = a_1 + \exp(a_2 + a_3 p + a_4 p^2). \quad (2)$$

The fit describes the data well: $\chi^2 = 70$ for 58 degrees of freedom. Above 2.8 GeV/ c , we observe $(36.7 \pm 0.2) \times 10^3$ events in the on-resonance data, compared to the fitted number of $(36.6 \pm 0.2) \times 10^3$ events.

2. $B\bar{B}$ Background

The electron spectrum from B -meson decays is composed of several contributions, dominated by the vari-

ous semileptonic decays. Hadronic B decays contribute mostly via hadron misidentification and secondary electrons from decays of D , J/ψ , and $\psi(2S)$ mesons.

We estimate the total background by fitting the observed inclusive electron spectrum to the sum of the signal and individual background contributions. For the individual signal and $B\bar{B}$ background contributions, we use the MC simulated spectra, and treat their relative normalization factors as free parameters in the fit. The non- $B\bar{B}$ background is parameterized by the exponential functions $f(\vec{a}, p_i)$, as described above. We expand the χ^2 definition as follows,

$$\chi^2 = \sum_i \frac{(f(\vec{a}, p_i) - r_L n_i)^2}{r_L^2 n_i} + \sum_j \frac{(f(\vec{a}, p_j) + S(\vec{b}, p_j) - N_j)^2}{N_j + \sigma_{j MC}^2}, \quad (3)$$

where the first sum is for the off-resonance data and the second sum for the on-resonance data. The $B\bar{B}$ electron spectrum is approximated as $S(\vec{b}, p_j) = \sum_k b_k g_k(p_j)$, where the free parameters b_k are the correction factors to the MC default branching fractions for the six individual contributions $g_k(p_j)$ representing the signal $B \rightarrow X_u e \nu$ decays, the background $B \rightarrow D e \nu$, $B \rightarrow D^* e \nu$, $B \rightarrow D^{**} e \nu$, $B \rightarrow D^{(*)} \pi e \nu$ decays, and the sum of other background events with electrons from secondary decays or misidentified hadrons. $\sigma_{j MC}$ is the statistical error of the number of simulated events in the j -th bin. The momentum spectra $g_k(p_j)$ are histograms taken from MC simulations.

3. Fit to Inclusive Spectra

The fit is performed simultaneously to the on- and off-resonance electron momentum spectra in the range from 1.1 to 3.5 GeV/ c , in bins of 50 MeV/ c . The lower part of the spectrum determines the relative normalization of the various background contributions, allowing for an extrapolation into the endpoint region above 2.0 GeV/ c . To reduce a potential systematic bias from the assumed shape of the signal spectrum, we combine the on-resonance data for the interval from 2.1 to 2.8 GeV/ c into a single bin. The lower limit of this bin is chosen so as to retain the sensitivity to the steeply falling $B\bar{B}$ background distributions, while containing a large fraction of the signal events in a region where the background is low. The fit results are insensitive to changes in this lower limit in the range of 2.0 to 2.2 GeV/ c . The number of signal events in a given momentum interval is taken as the excess of events above the fitted background.

The observed spectra, the fitted non- $B\bar{B}$ and $B\bar{B}$ backgrounds and the signal are shown and compared to MC simulations in Fig. 4. The fit has a χ^2 of 96 for 73 degrees of freedom. Above 2.3 GeV/ c , the non- $B\bar{B}$ background is dominant, while at low momenta the semileptonic $B\bar{B}$ background dominates. Contributions from

TABLE I: Summary of the signal extraction: the number of events (in units of 10^3) for the total sample, the principal background contributions, and the remaining signal, as well as the signal efficiencies, for five intervals of the electron momentum. The errors listed are statistical, including the uncertainties in the fitted scale factors for the non- $B\bar{B}$ and $X_c e\nu$ backgrounds.

Δp (GeV/c)	2.0 – 2.6	2.1 – 2.6	2.2 – 2.6	2.3 – 2.6	2.4 – 2.6
Total sample	609.81 ± 0.78	295.76 ± 0.54	133.59 ± 0.37	65.48 ± 0.26	35.38 ± 0.19
Non- $B\bar{B}$ background	142.38 ± 0.63	105.20 ± 0.48	74.86 ± 0.36	50.13 ± 0.25	29.96 ± 0.16
$X_c e\nu$ background	416.22 ± 2.52	157.17 ± 1.29	38.82 ± 0.47	4.00 ± 0.10	0.09 ± 0.01
J/ψ and $\psi(2S)$	6.17 ± 0.14	4.00 ± 0.10	2.33 ± 0.06	1.17 ± 0.04	0.47 ± 0.02
Other e^\pm background	1.61 ± 0.05	0.62 ± 0.02	0.24 ± 0.01	0.08 ± 0.01	0.03 ± 0.00
π mis-identification	1.34 ± 0.04	0.98 ± 0.03	0.64 ± 0.02	0.34 ± 0.02	0.10 ± 0.01
K mis-identification	0.47 ± 0.02	0.26 ± 0.01	0.13 ± 0.01	0.05 ± 0.01	0.01 ± 0.00
Other mis-identification	0.27 ± 0.01	0.15 ± 0.01	0.08 ± 0.01	0.04 ± 0.01	0.02 ± 0.00
$X_u e\nu$ background	1.62 ± 0.10	0.66 ± 0.05	0.20 ± 0.02	0.03 ± 0.01	0.01 ± 0.00
$X_u e\nu$ signal	39.72 ± 2.70	26.72 ± 1.49	16.31 ± 0.71	9.64 ± 0.38	4.70 ± 0.25
$X_u e\nu$ efficiency (%)	42.1 ± 0.3	41.2 ± 0.4	40.2 ± 0.5	39.5 ± 0.7	37.9 ± 1.0

hadron misidentification are small, varying from 6% to 4% as the electron momentum increases. The theoretical prediction for the signal $B \rightarrow X_u e\nu$ spectrum based on the BLNP calculations uses SF parameters extracted from the combined fit [27] to the moments measured by the BABAR Collaboration.

The fitting procedure was chosen in recognition of the fact that currently the branching fractions for the individual $B \rightarrow X_c \ell\nu$ decays are not well enough measured to perform an adequate background subtraction. The MC simulation takes into account the form factor and angular distributions for the $B \rightarrow D e\nu$ and $B \rightarrow D^* e\nu$ decays. For decays to higher-mass mesons, this information is not available. As a result, we do not consider this fit as a viable method of measuring these individual branching fractions. Nevertheless, the fitted branching fractions agree reasonably well with the measured branching fractions [32]. For the decays to higher-mass states, the ability of the fit to distinguish between decays to $D^{**} e\nu$ and $D^* \pi e\nu$ is limited. The sum of the two contributions, however, agrees with current measurements [32].

Table I shows a summary of the data, principal backgrounds and the resulting signal. The errors are statistical, but for the non- $B\bar{B}$ and $X_c e\nu$ background they include the uncertainties of the fitted parameters. The data are shown for five overlapping signal regions, ranging in width from 600 to 200 MeV/c. We therefore choose 2.6 GeV/c as the common upper limit of the signal regions because at higher momenta the signal contributions are very small compared to the non- $B\bar{B}$ background. As the lower limit is extended to 2.0 GeV/c, the error on the $B\bar{B}$ background subtraction increases.

IV. SYSTEMATIC ERRORS

A summary of the systematic errors is given in Table II for five intervals in the electron momentum. The principal systematic errors originate from the event selection and the background subtraction. The uncertainty in the

event simulation and its impact on the momentum dependence of the efficiencies for signal and background are the experimental limitations of the current analysis. The second largest source of uncertainties is the estimate of the $B\bar{B}$ background derived from the fit to the observed electron spectrum, primarily due to the uncertainties in the simulated momentum spectra of the various contributions. In addition, there are relatively small corrections to the momentum spectra due to variations in the beam energies, and radiative effects.

A. Detection and Simulation of $B \rightarrow X_u e\nu$ Decays

The selection efficiency for $B \rightarrow X_u e\nu$ decays is determined by MC simulation. We include in the uncertainty of the signal spectrum not only the uncertainty in the simulation of the detector response, but also the uncertainty in the simulation of the momentum and angular distributions of the electron, as well as the hadrons and the neutrino.

1. Detector related uncertainties

For a specific model of the signal decays there are three major factors that determine the efficiency: the track reconstruction for the electron, the electron identification, and losses due to the detector acceptance and event selection.

The uncertainty in the tracking efficiency has been studied in detail and is estimated to be $\sim 0.7\%$ per track. The average identification efficiency for electrons with momentum above 1.0 GeV/c is estimated to be on average 92% [29], based on large control samples of radiative Bhabha events and two-photon interactions. In $B\bar{B}$ events the actual efficiencies are slightly lower due to higher track and photon multiplicity. This difference decreases gradually from about 2.5% at 1.0 GeV/c to less than 0.8% at 2.0 GeV/c and above. We add in quadra-

TABLE II: Summary of the relative systematic errors (%) on the partial branching fraction measurements for $B \rightarrow X_u e \nu$ decays, as a function of p^{min} , the lower limit of the signal momentum range. The common upper limit is 2.6 GeV/c. The sensitivity of the signal extraction to the uncertainties in the SF parameters is listed as an additional systematic error, separately for the four sets of SF parameters.

p^{min} (GeV/c)	2.0	2.1	2.2	2.3	2.4
Track finding efficiency	0.7	0.7	0.7	0.7	0.7
Electron identification	1.4	1.4	1.3	0.9	0.8
Event selection efficiency	6.8	6.7	6.1	5.5	7.9
Non- $B\bar{B}$ background	2.4	2.5	2.4	2.5	2.3
J/ψ and $\psi(2S)$ background	0.9	0.8	0.8	0.6	0.5
$B \rightarrow D^* l \nu$ form factor	2.4	2.3	2.0	1.3	0.5
$B \rightarrow D l \nu$ form factor	0.7	0.9	0.8	0.2	0.4
$B \rightarrow D^{**} e \nu$ spectrum	2.8	2.5	2.4	0.9	0.7
Other e^\pm background	0.5	0.3	0.2	0.1	0.1
$B \rightarrow X_u e \nu$ background	1.1	0.6	0.3	0.1	0.0
π mis-identification background	0.8	0.9	0.9	0.8	0.5
K mis-identification background	0.4	0.4	0.3	0.2	0.1
Other hadron mis-identification	0.2	0.2	0.2	0.1	0.1
B movement	1.3	1.7	1.5	0.6	0.1
Bremsstrahlung and FSR	1.0	1.2	1.2	0.9	0.9
$N_{B\bar{B}}$ normalization	1.1	1.1	1.1	1.1	1.1
Total experimental error	8.8	8.6	7.9	6.6	8.5
$B \rightarrow X_u e \nu$ spectrum					
$X_s \gamma$ SF, fit to spectrum	6.0	3.5	1.6	0.3	0.1
$X_s \gamma$ SF, fit to moments	11.3	6.7	3.1	0.6	0.1
$X_c e \nu$ SF, fit to moments	13.3	8.6	4.0	0.8	0.0
SF, combined fit to moments	7.2	4.8	2.3	0.5	0.0
Total systematic error					
$X_s \gamma$ SF, fit to spectrum	10.7	9.3	8.1	6.6	8.5
$X_s \gamma$ SF, fit to moments	14.3	10.9	8.5	6.6	8.5
$X_c e \nu$ SF, fit to moments	15.9	12.2	8.9	6.6	8.5
SF, combined fit to moments	11.4	9.8	8.2	6.6	8.5

ture 50% of this observed difference to the statistical and systematic errors from the control samples. We assess the impact of this momentum-dependent uncertainty on the observed electron spectrum for both signal and background (see below).

2. Uncertainties in the signal spectrum

The momentum distribution of the signal electrons is not precisely known because many of the exclusive decay modes that make up the total inclusive $B \rightarrow X_u e \nu$ decays are still unobserved or poorly measured due to small event samples, and the form factors for most of the observed exclusive decay modes are not measured. To evaluate the sensitivity of the signal efficiency to the decay multiplicity and the shape of the momentum spectrum, we independently vary the relative contributions of the different decay modes by their current experimental uncertainties. We observe changes in the signal yield of less than 3.0% for the spectrum above 1.1 GeV/c, and less than 1.0% above 2.3 GeV/c.

The systematic uncertainties inherent in the modeling of the signal decays to non-resonant hadronic states and their impact on the signal yield have been studied by varying the SF parameters. We try four sets of SF parameters, two derived from the recent analysis of the $B \rightarrow X_s \gamma$ decays [25] based on the semi-inclusive photon spectrum and moments derived from this spectrum, one derived from moments in inclusive $B \rightarrow X_c l \nu$ decays [26], and one from a combined fit [27] to all moments measured by the *BABAR* Collaboration. For each set of SF parameters we calculate the signal momentum spectrum and repeat the fit to the data. We observe small changes in the fitted $B \rightarrow X_c l \nu$ background which result in changes of the signal yield. Taking into account the errors and correlations of the measured SF parameters, we derive the errors listed separately in Table II. The impact is largest for the signal regions extending to lower momenta, where this becomes the largest source of systematic error.

Not included in this estimate is the sensitivity of the signal yield to the event selection criteria, specifically those based on the variables \mathcal{R}_2 and p_{miss} . These selection criteria influence not only the signal, but more so the background distributions. Details are discussed below.

B. Non- $B\bar{B}$ Background

Systematic errors in the subtraction of the non- $B\bar{B}$ background could be introduced by the choice of the fitting function describing the electron spectrum and by the uncertainty in the relative normalization of the on- and off-resonance data.

To assess the uncertainty in the shape of this background we have compared fits with different parameterizations of the fit function. In addition to the exponential function described above (Eq. 2), we have tried linear combinations of Chebyshev polynomials up to fifth order. The resulting fits are equally consistent with the data. The differences in the non- $B\bar{B}$ background estimates between different parameterizations are less than 0.5%. Above 2.8 GeV/c the number of observed events in the on-resonance data sample agrees to 0.3% with the number of events predicted from the fit to the off-resonance sample.

If the relative normalization is treated as a free fit parameter, its deviation from the value based on luminosity measurements is less than one standard deviation. Thus, we use the more accurate value based on luminosity measurements. As a systematic error for the non- $B\bar{B}$ background we take 0.5% of this background contribution, which includes the errors of the normalization factor and the background shape approximation.

C. $B \rightarrow J/\psi X$ Background

J/ψ decays to e^+e^- pairs are vetoed by a restriction on the di-electron invariant mass. However, this veto is only about 50% efficient, primarily because of acceptance losses. The remaining, mostly single-electron background is estimated from simulation. We observe a difference of $(5.0 \pm 2.7)\%$ between the veto efficiency for electron pairs in data and simulation, and thus assign a 5% error to the residual background. This background amounts to 18% of the signal for $p_e > 2.0$ GeV/ c and 10% for $p_e > 2.3$ GeV/ c and the resulting uncertainty on the signal branching fraction is estimated to vary from 0.9% to 0.5%. The background from $\psi(2S) \rightarrow e^+e^-$ decays is significantly smaller, and thus its uncertainty is negligible.

D. $B\bar{B}$ Background

The shapes of the $B\bar{B}$ backgrounds are derived from MC simulations. The branching fractions for exclusive semileptonic $B \rightarrow X_c e \nu$ decays are currently not precisely known. Thus the electron spectra from inclusive $B \rightarrow X_c e \nu$ decays may differ from those of the simulation. For this reason, we have introduced scale factors in the fits to the electron spectrum to adjust the relative normalization of the various contributions. To test the sensitivity to the shape of the dominant contributions, we have varied the form factors for decays to $D^* e \nu$ and $De \nu$, and changed the relative proportion of contributions from narrow and wide resonances to $D^{**} e \nu$ decays.

For $B \rightarrow De \nu$ and $B \rightarrow D^* e \nu$ decays we use HQET parameterizations [36, 37] of the form factors. To study the impact of the uncertainties in the measured form factors, we reweight the MC-simulated spectrum for a given decay mode to reproduce the change in the spectrum due to variations of the form-factor parameters, and repeat the standard fit to the data. From the observed changes in the signal yield as a function of the choice of the form-factor parameters for $D^* e \nu$ decays, we assess the systematic error on the signal yield by taking into account the measured form-factor parameters, ρ^2 , R_1 , and R_2 , their errors, and their covariance matrix [40]. For $De \nu$ decays, we rely on a measurement of ρ_D^2 by the CLEO [38] and Belle Collaborations [39]. Similarly, we estimate the impact of the uncertainty in ρ_D^2 by comparing the default fit results with spectra corresponding to variations of ρ_D^2 by one standard deviation. We take the shift of the signal yield as a systematic error.

To assess the impact of the poorly known branching fractions for various $D^{**} e \nu$ decay modes on the shape of the electron spectrum, we have repeated the fits with the relative branching fractions for the individual decay modes changed by up to 50%. As long as we do not eliminate the decays to the two narrow resonances, $D_1(2437)$ and $D_2(2459)$, we obtain consistent results. Specifically, if we eliminate the decays involving the two wider res-

onances, $D_0(2308)$ and $D_1'(2460)$, the results change by less than 3%. We adopt this change as the estimate of the systematic error due to the uncertainty of decays to D^{**} states.

Similarly, we vary the branching fractions for secondary electrons from semileptonic D decays by 10% and adopt the observed change as a systematic error. In addition, there is a small contribution from events which contain a $B \rightarrow X_u e \nu$ decay, but contribute to the background rather than the signal, because the track identified as a signal electron does not originate from this decay. We estimate the uncertainty of this very small contribution to be 30%.

For background from hadronic B decays, the uncertainty in the spectrum is primarily due to the uncertainty in the momentum-dependent hadron misidentification. The uncertainties of misidentification probabilities are estimated to be 20% and 30%, for pions and kaons, respectively. The uncertainty in the fractions of pions and kaons is taken as the difference between simulated and observed charged particle spectra, which is about 5% for pions and kaons. With these uncertainties in the hadron misidentification backgrounds, the fractional error in the number of subtracted background events is $\sim 20\%$ for pions and $\sim 30\%$ for kaons. In addition, there is a small background from protons and from unidentified particles; its total uncertainty is estimated to be about 50% smaller than for identified kaons.

E. Uncertainty in the B Meson Momentum Spectrum

The non-zero momentum of the B meson in the $\Upsilon(4S)$ rest frame affects the shape of the electron spectrum near the endpoint. To estimate the systematic error associated with the uncertainty in the initial B -meson momentum spectrum, we compare the simulated and measured energy spectra for fully reconstructed charged B mesons for different data taking periods. The widths of the energy distributions agree well for all data, but in some of the data sets we observed a shift in the central value of up to 2.2 MeV relative to the simulation, which assumes a fixed center-of-mass energy. We correct the simulation for the observed shifts, and assess the effect of the uncertainty of 0.13 MeV in this shift on the branching fraction measurement.

F. Bremsstrahlung and Radiative Corrections

For comparison with other experiments and with theoretical calculations, the signal spectrum resulting from the fit is corrected for bremsstrahlung in the detector and for final-state radiation. Corrections for QED radiation in the decay process are simulated using PHOTOS [31]. This simulation includes multiple-photon emission from the electron, but does not include electroweak correc-

tions for quarks. The accuracy of this simulation has been compared to analytical calculations performed to $\mathcal{O}(\alpha)$ [31]. Based on this comparison we assign an uncertainty of 20% to the PHOTOS correction, leading to an uncertainty in the signal yield of about 1%.

The uncertainty in the energy loss of electrons due to bremsstrahlung in the beam pipe and tracking system is determined by the uncertainty in the thickness of the detector material, estimated to be $(0.0450 \pm 0.0014)X_0$ at normal incidence. The thickness of the material was verified using electrons from Bhabha scattering as a function of the polar angle relative to the beam. The impact of the uncertainty in the energy loss on the signal rate was estimated by calculating the impact of an additional $0.0014X_0$ of material.

G. Sensitivity to the Event Selection

We have checked the sensitivity of the fits to the electron spectrum to changes in the event selection. We have also assessed the impact of the momentum-dependent uncertainty in the electron efficiency on the fitted signal yield. These variations of the event selection change the signal efficiency and lead to variations of up to 50% in the size of the non- $B\bar{B}$ background, and up to 20% in the $B\bar{B}$ background.

Though some of the observed changes in the efficiency-corrected signal yield may already be covered by the form-factor and other variations, we conclude that these tests do reveal significant changes that have to be accounted for.

The largest variation (5%) is observed for changes in the restriction on ratio of the Fox-Wolfram moments, \mathcal{R}_2 , from the default value of 0.5 to 0.6. Other sizable variations are observed for changes in the restrictions on the absolute value and direction of the missing momentum vector. \mathcal{R}_2 and the missing momentum are quantities that are derived from the measured momenta of all charged and neutral particles in the event, and are therefore sensitive to even small differences in data and simulation. We interpret the observed changes as representative for the uncertainties in the MC simulation of the selection of signal and background events and adopt the observed changes between the default fits and the fits with looser selection criteria as systematic errors. Adding the observed changes in quadrature leads to a relative systematic error of between 5% and 8% on the partial branching fraction.

V. RESULTS

A. Determination of the Partial $B \rightarrow X_u e \nu$ Branching Fraction

For a given interval Δp in the electron momentum, we calculate the inclusive partial branching fraction $B \rightarrow$

$X_u e \nu$ according to

$$\Delta\mathcal{B}(\Delta p) = \frac{N_{tot}(\Delta p) - N_{bg}(\Delta p)}{2\epsilon(\Delta p)N_{B\bar{B}}} (1 + \delta_{rad}(\Delta p)). \quad (4)$$

Here N_{tot} refers to the total number of electron candidates selected in the on-resonance data and N_{bg} refers to the total background, from non- $B\bar{B}$ and $B\bar{B}$ events, as determined from the fit to the spectrum. $\epsilon(\Delta p)$ is the total efficiency for selecting a signal electron from $B \rightarrow X_u e \nu$ decays (including bremsstrahlung in the detector material), and δ_{rad} accounts for the distortion of the electron spectrum due to final-state radiation. This is a momentum-dependent correction, derived from the MC simulation based on PHOTOS [31]. The total number of produced $B\bar{B}$ events is $N_{B\bar{B}} = (88.36 \pm 0.02_{stat} \pm 0.97_{syst}) \times 10^6$.

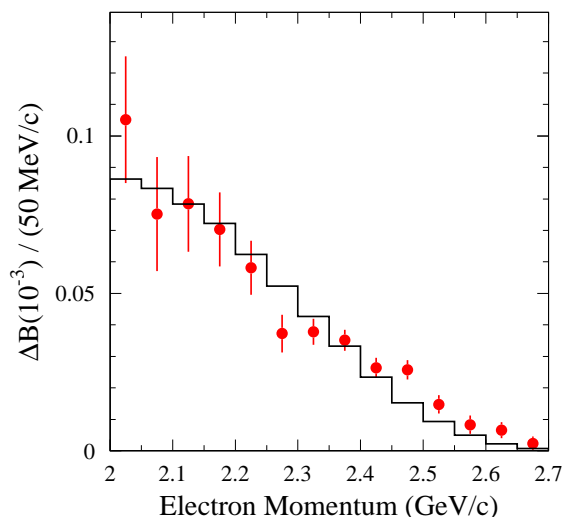


FIG. 5: The differential branching fraction for charmless semileptonic B decays (data points) as a function of the electron momentum (in the $\Upsilon(4S)$ rest frame) after background subtraction and corrections for bremsstrahlung and final state radiation, compared to the Monte Carlo simulation (histogram). The errors indicate the statistical errors on the background subtraction, including the uncertainties of the fit parameters. For the signal simulation, the SF parameters are extracted from a combined fit to all $BABAR$ moments.

The differential branching fraction as a function of the electron momentum in the $\Upsilon(4S)$ rest frame is shown in Fig. 5, fully corrected for efficiencies and radiative effects. The data are well reproduced by the signal simulations using the SF parameters derived from the combined fit to all moments measured by the $BABAR$ Collaboration [27], specifically $m_b^{SF}(1.5 \text{ GeV}) = 4.59 \text{ GeV}/c^2$, $\mu_\pi^{2SF}(1.5 \text{ GeV}) = 0.21 \text{ GeV}^2$. The partial branching fractions for the five overlapping electron momentum intervals are summarized in Table III. The stated errors on $\Delta\mathcal{B}$ represent the statistical and total systematic uncertainties of the measurement, including the uncertainty

due to the sensitivity to the SF parameters, as stated in Table II. As the lower limit on the electron momentum decreases, the statistical and systematic errors are more and more dominated by the $B \rightarrow X_c e \nu$ background subtraction.

B. Extraction of the Total Charmless Branching Fraction and $|V_{ub}|$

As mentioned earlier, we use two sets of theoretical calculations to extract $|V_{ub}|$ from the partial electron spectrum. The first, and so far the most commonly used, method derives $|V_{ub}|$ from the total charmless semileptonic branching fraction and the average B lifetime, $\tau_b = (1.604 \pm 0.012)$ ps [49], as follows,

$$|V_{ub}| = 0.00424 \left(\frac{\mathcal{B}(B \rightarrow X_u l \nu)}{0.002} \frac{1.61 \text{ ps}}{\tau_b} \right)^{1/2} \times (1.0 \pm 0.028_{\text{pert}+\text{nonpert}} \pm 0.039_{m_b}). \quad (5)$$

Here the first error represents the linear sum of the uncertainties of the perturbative and non-perturbative QCD corrections, and the second error is due to the uncertainty in m_b . An overall correction of 0.7% is included to account for QED corrections. This formulation [46–48] has been updated to take into account the recent measurement [26] of m_b , μ_π^2 , and other parameters of the heavy quark expansion in the kinetic mass scheme, specifically $m_b^{\text{kin}}(1.0 \text{ GeV}) = (4.61 \pm 0.07) \text{ GeV}/c^2$ and $\mu_\pi^{2(\text{kin})}(1.0 \text{ GeV}) = (0.45 \pm 0.05) \text{ GeV}^2$.

We determine the total branching fraction,

$$\mathcal{B}(B \rightarrow X_u e \nu) = \Delta\mathcal{B}(\Delta p)/f_u(\Delta p), \quad (6)$$

where $f_u(\Delta p)$ is the fraction of the electron spectrum in a given momentum interval Δp . The values of $f_u(\Delta p)$ are estimated based on the DN calculations [17] using the exponential parameterization of the SF, with the SF parameters extracted from fits to the photon spectrum in semi-inclusive $B \rightarrow X_s \gamma$ decays, as measured by the *BABAR* Collaboration [25], $\bar{\Lambda}^{SF} = (0.49_{-0.06}^{+0.10}) \text{ GeV}/c^2$, $\lambda_1^{SF} = (-0.24_{-0.18}^{+0.09}) \text{ GeV}^2$, with a correlation coefficient of -0.94 . We obtain very similar results for the two other functional forms suggested to describe the SF [17].

The results for the predicted fraction $f_u(\Delta p)$, the total charmless branching fraction, \mathcal{B} , and $|V_{ub}|$ are presented in Table III. The first error on f_u refers to the experimental error of the SF parameters from the measurement of the inclusive photon spectrum. It includes the uncertainty of the background subtraction and the extrapolation to decays to unmeasured X_s states. We have taken into account the stated error of the SF parameters, including their correlation. Specifically, we have taken as an error on $f_u(\Delta p)$ the maximum deviation of the $f_u(\Delta p)$ from its central value for selected values of the SF parameters on the error ellipse. The second error accounts for the dependence on the α_s scale, for the uncertainty in the

form of the SF, and for the uncertainty in the theoretical prediction of f_u from the $B \rightarrow X_s \gamma$ measurement. As suggested by DN [50] this error has been estimated by varying the values of $\bar{\Lambda}^{SF}$ and λ_1^{SF} by 10%.

The errors listed for \mathcal{B} and $|V_{ub}|$ are specified as follows. The first error reflects the error on the measurement of $\Delta\mathcal{B}$, which includes statistical and experimental systematic uncertainties, except for the uncertainty in the SF parameters. The second error is due to experimental uncertainty of SF parameters affecting both $f_u(\Delta p)$ and $\Delta\mathcal{B}$. The third error is the theoretical uncertainty of $f_u(\Delta p)$. The fourth error on $|V_{ub}|$ accounts for the theoretical uncertainty in the translation from \mathcal{B} to $|V_{ub}|$, as specified in Eq. 5. This error also depends on the b -quark mass and thus is correlated with the theoretical uncertainty on the SF.

The results for the total branching fraction \mathcal{B} and $|V_{ub}|$ obtained from the different momentum intervals are consistent within the experimental and theoretical uncertainties. For intervals extending below $2.3 \text{ GeV}/c$, the total errors on \mathcal{B} and $|V_{ub}|$ do not depend very strongly on the chosen momentum interval. While the errors on $\Delta\mathcal{B}$ are smallest above the kinematic endpoint for $B \rightarrow X_c e \nu$ decays, the dominant uncertainty arises from the determination of the fraction f_u and increases substantially with higher momentum cut-offs. The stated theoretical errors on f_u , acknowledged as being underestimated [50], do not include uncertainties from weak annihilation and other power-suppressed corrections. Assuming that one can combine the experimental and theoretical errors in quadrature, the best measurement of the total branching fraction is obtained for the momentum interval $2.0 - 2.6 \text{ GeV}/c$.

Though the *BABAR* measurement of the photon spectrum [25] results in the best estimate for the SF parameters, we have also considered sets of SF parameters obtained from photon spectra measured by the CLEO [51] and Belle [52] Collaborations. These parameters are listed in Table IV. In Table V the results obtained for these different SF parameters based on the *BABAR* semileptonic data and on the DN calculations are listed for the momentum interval $2.0 - 2.6 \text{ GeV}/c$. The values of the SF parameters obtained by the CLEO Collaboration agree very well with the *BABAR* results, while they differ from the values obtained by the Belle Collaboration, though the differences are comparable to the experimental errors on these parameters. The differences affect the signal spectrum, and thereby the fitted background yield. These differences are largest for the lower end of the signal region and vanish for the high momentum intervals. The impact of the SF parameters on the partial branching fractions is included in the total error (see Table II).

The second method for extracting $|V_{ub}|$ is based on recent BLNP calculations [24]. In this framework the partial branching fraction $\Delta\mathcal{B}$ is related directly to $|V_{ub}|$:

$$|V_{ub}| = \sqrt{\frac{\Delta\mathcal{B}}{\tau_b \zeta(\Delta p)}}, \quad (7)$$

TABLE III: The partial ($\Delta\mathcal{B}$) and total (\mathcal{B}) branching fraction for inclusive $B \rightarrow X_u e \nu$ decays and $|V_{ub}|$ for five electron momentum intervals. The spectral fractions f_u are determined using SF parameters extracted from a fit to the photon spectrum in $B \rightarrow X_s \gamma$ decays [25] based on calculations by DeFazio and Neubert [17] and Kagan and Neubert [18]. The errors are explained in the text.

Δp (GeV/c)	$\Delta\mathcal{B}(10^{-3})$	$f_u(\Delta p)$	$\mathcal{B}(10^{-3})$	$ V_{ub} (10^{-3})$
2.0 – 2.6	$0.479 \pm 0.033 \pm 0.050$	$0.298 \pm 0.029 \pm 0.015$	$1.61 \pm 0.18 \pm 0.25 \pm 0.08$	$3.80 \pm 0.21 \pm 0.29 \pm 0.10 \pm 0.18$
2.1 – 2.6	$0.350 \pm 0.020 \pm 0.033$	$0.222 \pm 0.026 \pm 0.016$	$1.58 \pm 0.16 \pm 0.24 \pm 0.11$	$3.77 \pm 0.19 \pm 0.28 \pm 0.13 \pm 0.18$
2.2 – 2.6	$0.231 \pm 0.010 \pm 0.018$	$0.149 \pm 0.020 \pm 0.016$	$1.55 \pm 0.14 \pm 0.23 \pm 0.16$	$3.73 \pm 0.17 \pm 0.27 \pm 0.19 \pm 0.18$
2.3 – 2.6	$0.146 \pm 0.006 \pm 0.010$	$0.086 \pm 0.013 \pm 0.013$	$1.71 \pm 0.13 \pm 0.25 \pm 0.26$	$3.92 \pm 0.15 \pm 0.29 \pm 0.30 \pm 0.19$
2.4 – 2.6	$0.075 \pm 0.004 \pm 0.006$	$0.039 \pm 0.006 \pm 0.009$	$1.95 \pm 0.20 \pm 0.32 \pm 0.45$	$4.18 \pm 0.21 \pm 0.35 \pm 0.48 \pm 0.20$

TABLE IV: SF parameters (at a scale of 1.5 GeV) measured by different experiments, based on two different theoretical calculations, top: DN [17, 18], bottom: BLNP [24].

Experiment	SF Input	$\bar{\Lambda}$ (GeV/c ²)	λ_1 (GeV ²)
BABAR	(spectrum) $X_s \gamma$ [25]	$0.49^{+0.10}_{-0.06}$	$-0.24^{+0.09}_{-0.18}$
CLEO	(spectrum) $X_s \gamma$ [51]	$0.54^{+0.26}_{-0.11}$	$-0.34^{+0.18}_{-0.88}$
Belle	(spectrum) $X_s \gamma$ [52]	$0.66^{+0.09}_{-0.06}$	$-0.40^{+0.17}_{-0.32}$
Experiment	SF Input	$\bar{\Lambda}$ (GeV/c ²)	μ_π^2 (GeV ²)
BABAR	(spectrum) $X_s \gamma$ [25]	$0.61^{+0.07}_{-0.07}$	$0.16^{+0.10}_{-0.08}$
BABAR	(moments) $X_s \gamma$ [25]	$0.75^{+0.11}_{-0.13}$	$0.35^{+0.11}_{-0.15}$
BABAR	(moments) $X_c \ell \nu$ [26]	0.67 ± 0.08	0.15 ± 0.07
BABAR	(comb. moments) [27]	0.69 ± 0.05	0.21 ± 0.05

where $\zeta(\Delta p)$ is the prediction for the partial rate for $B \rightarrow X_u e \nu$ decays (in units of ps⁻¹). In these calculations the leading order SF is constrained by the HQE parameters, obtained either from the $B \rightarrow X_s \gamma$ or $B \rightarrow X_c e \nu$ decays, or both.

The values of the SF parameters extracted from the BABAR analyses of inclusive $B \rightarrow X_s \gamma$ [25], $B \rightarrow X_c e \nu$ [26] decays, and the combined fit [27] to all moments measured by the BABAR Collaboration are listed in Table IV. Note that the definitions of shape functions and the SF parameters are different for the DN and BLNP calculations. The different SF parameters and their measurement errors are also shown in Fig. 6.

The SF parameters based on $B \rightarrow X_s \gamma$ data only are extracted from either a fit to the photon spectrum or to the first and second moments of this spectrum in the “shape function” scheme. The HQE parameters extracted from fits to measured moments in the kinetic mass scheme have been translated into the “shape function” scheme at the appropriate scale. Specifically, the HQE parameters extracted from the moments in $B \rightarrow X_c e \nu$ decays have been translated based on two-loop calculations [23]. The HQE parameters resulting from the combined fit to moments of the photon, lepton, and hadron mass spectra in the kinetic scheme are used to predict the first and second moments of the photon spectrum down to photon energies of 1.6 GeV, based on cal-

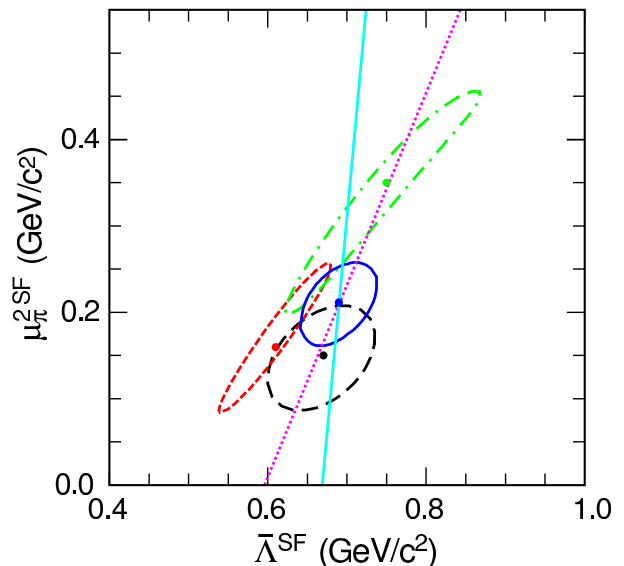


FIG. 6: (color online) The fitted values and contours corresponding to $\Delta\chi^2 = 1$ for the four sets of SF parameters (see Table IV) based on the calculations of BLNP, extracted from the photon energy spectrum (short dash - red) and from the photon energy moments (dot-dash - green) in $B \rightarrow X_s \gamma$, from the lepton energy and hadron mass moments in $B \rightarrow X_c e \nu$ decays (long dash - black), as well as from the combined fit to moments (solid - blue) measured by the BABAR Collaboration. Also shown are two straight lines indicating values of the SF parameters, for which the partial branching fraction (dotted - magenta) and $|V_{ub}|$ (solid - light blue) are constant.

culations by Benson, Bigi, and Uraltsev [53]. The lower limit on the photon energy is chosen such that the estimated cut-induced perturbative and non-perturbative corrections to the HQE are negligible. From these predicted moments, the SF parameters are extracted using the next-to-leading order calculations in a framework that is consistent with the one used for the determination of $|V_{ub}|$ [24].

The smallest errors on the SF parameters are obtained from the fit to the photon spectrum and the combined fit to all moments. The fit to the photon spectrum is most sensitive to the high end of the photon energy spectrum, and relies on the theoretical prediction for the shape of

TABLE V: Comparison of measurements of the partial ($\Delta\mathcal{B}$) and total (\mathcal{B}) branching fraction for inclusive $B \rightarrow X_u e \nu$ decays and $|V_{ub}|$ for the electron momentum interval 2.0 to 2.6 GeV/c. The results are obtained for SF parameters (listed in Table IV) extracted from different experiments. The first three measurements are based on DN [17, 18] calculations, the remaining four on BLNP [24] calculations, based on SF parameters extracted from the photon spectra and energy moments, the $B \rightarrow X_c \ell \nu$ moments [26], and a combined fit to moments [27]. The errors are explained in the text.

Experiment	SF input	$\Delta\mathcal{B} (10^{-3})$	$\mathcal{B} (10^{-3})$	$ V_{ub} (10^{-3})$
<i>BABAR</i>	$X_s \gamma$ (spectrum)	$0.479 \pm 0.033 \pm 0.050$	$1.61 \pm 0.18 \pm 0.25 \pm 0.08$	$3.80 \pm 0.21 \pm 0.29 \pm 0.10 \pm 0.18$
CLEO	$X_s \gamma$ (spectrum)	$0.491 \pm 0.036 \pm 0.061$	$1.75 \pm 0.20 \pm 0.48 \pm 0.11$	$3.97 \pm 0.23 \pm 0.54 \pm 0.12 \pm 0.19$
Belle	$X_s \gamma$ (spectrum)	$0.548 \pm 0.038 \pm 0.057$	$2.24 \pm 0.25 \pm 0.27 \pm 0.20$	$4.48 \pm 0.25 \pm 0.27 \pm 0.20 \pm 0.22$
<i>BABAR</i>	$X_s \gamma$ (spectrum)	$0.514 \pm 0.037 \pm 0.055$	$1.81 \pm 0.20 \begin{smallmatrix} +0.32 \\ -0.24 \end{smallmatrix} \pm 0.11$	$3.80 \pm 0.21 \begin{smallmatrix} +0.49 \\ -0.39 \end{smallmatrix} \pm 0.18$
<i>BABAR</i>	$X_s \gamma$ (moments)	$0.577 \pm 0.041 \pm 0.082$	$2.57 \pm 0.29 \begin{smallmatrix} +1.16 \\ -0.66 \end{smallmatrix} \pm 0.23$	$4.86 \pm 0.28 \begin{smallmatrix} +1.20 \\ -0.89 \end{smallmatrix} \pm 0.26$
<i>BABAR</i>	$X_c \ell \nu$ (moments)	$0.569 \pm 0.039 \pm 0.090$	$2.17 \pm 0.24 \begin{smallmatrix} +0.58 \\ -0.41 \end{smallmatrix} \pm 0.15$	$4.30 \pm 0.24 \begin{smallmatrix} +0.75 \\ -0.59 \end{smallmatrix} \pm 0.21$
<i>BABAR</i>	combined fit to moments	$0.572 \pm 0.041 \pm 0.065$	$2.27 \pm 0.26 \begin{smallmatrix} +0.33 \\ -0.28 \end{smallmatrix} \pm 0.17$	$4.44 \pm 0.25 \begin{smallmatrix} +0.42 \\ -0.38 \end{smallmatrix} \pm 0.22$

the spectrum down to low photon energies. Since this shape is not directly calculable, several forms of the SF are used to assess the uncertainty of this approach. The use of two sets of the first and second moments of the photon spectrum, above 1.90 and above 2.09 GeV, is less powerful, due to much larger statistical and systematic errors, but insensitive to the theoretical knowledge of the detailed shape of the spectrum. The SF parameters obtained from moments of the photon spectrum above 1.90 GeV/c agree with those obtained from the global fit to the moments, but also have larger errors. Nevertheless, the inclusion of the photon energy moments significantly improves the sensitivity of the global fit to more than 30 measured moments.

The results for the partial branching fractions $\Delta\mathcal{B}$ and $|V_{ub}|$ based on the BLNP calculations are listed in Tables VI, VII, VIII, and IX for the four sets of SF parameters.

The errors cited in these tables are defined and determined in analogy to those in Table III. The first error on the predicted rate ζ accounts for the uncertainty due to the errors in measured parameters of the leading SF, the second error refers to the theoretical uncertainties in the subleading SFs, and variations of scale matching, as well as weak annihilation effects. For $|V_{ub}|$, the first error is the experimental error on the partial branching fraction, which includes the statistical and the experimental systematic uncertainty, the second error includes systematic uncertainties on the partial branching fraction and ζ due to the uncertainty of the SF parameters, and the third error is the theoretical uncertainty on ζ , estimated using the prescription suggested by BLNP.

In Table V the results obtained for these different SF parameters based on the *BABAR* semileptonic data and on the BLNP (and DN) calculations are listed for the momentum interval 2.0 – 2.6 GeV/c. The observed differences are consistent with the total error stated; they are largest for the SF parameters extracted from the fit to the photon spectrum as compared to the moments of the photon spectrum.

For all four sets of SFs we observe a tendency for the total branching fraction, and therefore also $|V_{ub}|$, to be slightly larger at the higher momentum intervals, but the uncertainties in the predicted rates ζ are very large for the highest momentum interval.

Based on the BLNP calculations [24] of the inclusive lepton spectra, we have also determined the total $B \rightarrow X_u e \nu$ branching fraction. The results are presented in Table X.

The results for $|V_{ub}|$ extracted for the BLNP calculations are close to those obtained for the DN calculations (see Table V). In fact, the results based on the fit to the photon spectrum measured by the *BABAR* Collaboration are identical for all electron momentum ranges, even though the partial branching fractions differ by one standard deviation of the experimental error (see Tables III and VI). Changing the ansatz for the SF from the exponential to a hyperbolic function [24] has no impact on the results.

VI. CONCLUSIONS

In summary, we have measured the inclusive electron spectrum in charmless semileptonic B decays and derived partial branching fractions in five overlapping electron momentum intervals close to the kinematic endpoint. We have extracted the partial and total branching fractions and the magnitude of the CKM element $|V_{ub}|$ based on two sets of calculations: the earlier ones by DeFazio and Neubert [17] and Kagan and Neubert [18], and the more comprehensive calculations by Lange, Neubert and Paz [24], as summarized in Table V. Within the stated errors, the measurements in the different momentum intervals are consistent for both sets of calculations.

We adopt the results based on the more recent calculations (BLNP) [24], since they represent a more complete theoretical analysis of the full electron spectrum and relate the SF to the HQE parameters extracted from inclusive $B \rightarrow X_s \gamma$ and $B \rightarrow X_c \ell \nu$ decays. We choose the SF

TABLE VI: The partial branching fraction $\Delta\mathcal{B}$, the predicted partial rate ζ for $B \rightarrow X_u e \nu$ decays and $|V_{ub}|$ for five electron momentum intervals, using the SF parameters from the photon spectrum in semi-inclusive $B \rightarrow X_s \gamma$ decays, ($\bar{\Lambda}^{SF} = (0.61^{+0.07}_{-0.07}) \text{ GeV}/c^2$, $\mu_\pi^{2SF} = (0.16^{+0.10}_{-0.08}) \text{ GeV}^2$, fit to spectrum) [25] based on BLNP calculations [24]. The errors are explained in the text.

Δp (GeV/c)	$\Delta\mathcal{B} (10^{-3})$	$\zeta(\Delta p)(\text{ps}^{-1})$	$ V_{ub} (10^{-3})$
2.0 – 2.6	$0.514 \pm 0.037 \pm 0.055$	$22.2 \pm 3.9 \pm 2.1$	$3.80 \pm 0.21 \begin{smallmatrix} +0.49 \\ -0.39 \end{smallmatrix} \pm 0.18$
2.1 – 2.6	$0.366 \pm 0.021 \pm 0.034$	$16.1 \pm 3.3 \pm 1.7$	$3.76 \pm 0.20 \begin{smallmatrix} +0.49 \\ -0.39 \end{smallmatrix} \pm 0.20$
2.2 – 2.6	$0.236 \pm 0.011 \pm 0.019$	$10.5 \pm 2.4 \pm 1.5$	$3.75 \pm 0.17 \begin{smallmatrix} +0.49 \\ -0.40 \end{smallmatrix} \pm 0.27$
2.3 – 2.6	$0.147 \pm 0.006 \pm 0.010$	$5.8 \pm 1.5 \pm 1.6$	$3.98 \pm 0.16 \begin{smallmatrix} +0.53 \\ -0.43 \end{smallmatrix} \pm 0.55$
2.4 – 2.6	$0.075 \pm 0.004 \pm 0.006$	$2.5 \pm 0.7 \pm 2.1$	$4.32 \pm 0.22 \begin{smallmatrix} +0.59 \\ -0.49 \end{smallmatrix} \pm 1.81$

TABLE VII: The partial branching fraction $\Delta\mathcal{B}$, the predicted partial rate ζ for $B \rightarrow X_u e \nu$ decays and $|V_{ub}|$ for five electron momentum intervals, using the SF parameters from the moments of the photon energy spectrum in semi-inclusive $B \rightarrow X_s \gamma$ decays, ($\bar{\Lambda}^{SF} = (0.75^{+0.11}_{-0.13}) \text{ GeV}/c^2$, $\mu_\pi^{2SF} = (0.35^{+0.11}_{-0.15}) \text{ GeV}^2$, fit to moments) [25] based on BLNP calculations [24]. The errors are explained in the text.

Δp (GeV/c)	$\Delta\mathcal{B} (10^{-3})$	$\zeta(\Delta p)(\text{ps}^{-1})$	$ V_{ub} (10^{-3})$
2.0 – 2.6	$0.577 \pm 0.041 \pm 0.082$	$15.2 \pm 5.1 \pm 1.6$	$4.86 \pm 0.28 \begin{smallmatrix} +1.20 \\ -0.89 \end{smallmatrix} \pm 0.26$
2.1 – 2.6	$0.392 \pm 0.024 \pm 0.043$	$10.5 \pm 4.1 \pm 1.5$	$4.82 \pm 0.25 \begin{smallmatrix} +1.20 \\ -0.88 \end{smallmatrix} \pm 0.33$
2.2 – 2.6	$0.243 \pm 0.011 \pm 0.021$	$6.5 \pm 3.0 \pm 1.4$	$4.82 \pm 0.22 \begin{smallmatrix} +1.24 \\ -0.89 \end{smallmatrix} \pm 0.52$
2.3 – 2.6	$0.148 \pm 0.006 \pm 0.010$	$3.5 \pm 1.8 \pm 1.6$	$5.15 \pm 0.20 \begin{smallmatrix} +1.39 \\ -0.98 \end{smallmatrix} \pm 1.20$
2.4 – 2.6	$0.075 \pm 0.004 \pm 0.006$	$1.5 \pm 0.8 \begin{smallmatrix} +2.3 \\ -1.5 \end{smallmatrix}$	$5.62 \pm 0.29 \begin{smallmatrix} +1.61 \\ -1.14 \end{smallmatrix} \pm 4.27$

parameters obtained from the combined fit to moments of inclusive distributions measured by the *BABAR* Collaboration rather than the single most precise measurement of the SF parameters obtained from the recent *BABAR* measurement [25] of the semi-inclusive photon spectrum in $B \rightarrow X_s \gamma$ decays. Assuming it is valid to combine the experimental and the estimated theoretical errors in quadrature, and taking into account the fraction of the signal contained in this interval, we conclude that the best measurement can be extracted from the largest momentum interval, 2.0 to 2.6 GeV/c. For this momentum interval the partial branching fraction is

$$\Delta\mathcal{B}(B \rightarrow X_u e \nu) = (0.572 \pm 0.041_{stat} \pm 0.065_{syst}) \times 10^{-3}. \quad (8)$$

Here the first error is statistical and the second is the total systematic error, as listed in Table II. In addition to the systematic uncertainty due to the signal extraction, the normalization, and various small corrections, this error also includes the observed dependence of the extracted signal on the choice of the SF parameters. Based on the BLNP method, we obtain a total branching fraction of

$$\mathcal{B}(B \rightarrow X_u e \nu) = (2.27 \pm 0.26_{exp} \begin{smallmatrix} +0.33 \\ -0.28 \end{smallmatrix} SF \pm 0.17_{theory}) \times 10^{-3}, \quad (9)$$

and

$$|V_{ub}| = (4.44 \pm 0.25_{exp} \begin{smallmatrix} +0.42 \\ -0.38 \end{smallmatrix} SF \pm 0.22_{theory}) \times 10^{-3}. \quad (10)$$

Here the first error represents the total experimental uncertainty, the second refers to the uncertainty in the SF parameters from the combined fit to moments, and the third combines the stated theoretical uncertainties in the extraction of $|V_{ub}|$, including uncertainties from the sub-leading SFs, weak annihilation effects, and various scale-matching uncertainties. No additional uncertainty due to the theoretical assumption of quark-hadron duality has been assigned.

The improvement in precision compared to earlier analyses of the lepton spectrum near the kinematic endpoint can be attributed to improvements in experimental techniques, to higher statistics, and in particular, to improved background estimates, as well as significant advances in the theoretical understanding of the SFs and extraction of the SF parameters from inclusive spectra and moments. While earlier measurements were restricted to lepton energies close to the kinematic endpoint for $B \rightarrow X_c \ell \nu$ decays at 2.3 GeV/c and covered only 10% of the $B \rightarrow X_u \ell \nu$ spectrum, these and other more recent measurements have been extended to lower momenta, including about 25% of the spectrum, and thus have resulted in a significant reduction in the theoretical uncertainties on $|V_{ub}|$.

The determination of $|V_{ub}|$ is currently limited primarily by our knowledge of SF parameters. An approximate linear dependence of $|V_{ub}|$ on these parameters is

$$\frac{\Delta|V_{ub}|}{|V_{ub}|} = 1.31 \frac{\Delta\bar{\Lambda}}{\bar{\Lambda}} - 0.04 \frac{\Delta\mu_\pi^2}{\mu_\pi^2}. \quad (11)$$

TABLE VIII: The partial branching fraction $\Delta\mathcal{B}$, the predicted partial rate ζ for $B \rightarrow X_u e \nu$ decays and $|V_{ub}|$ for five electron momentum intervals, based on the SF parameters from hadron mass and lepton moments in $B \rightarrow X_c e \nu$ decays ($\bar{\Lambda}^{SF} = (0.67 \pm 0.08) \text{ GeV}/c^2$, $\mu_\pi^{2SF} = (0.15 \pm 0.07) \text{ GeV}^2$) [26] based on BLNP calculations [24]. The errors are explained in the text.

Δp (GeV/c)	$\Delta\mathcal{B} (10^{-3})$	$\zeta(\Delta p)(\text{ps}^{-1})$	$ V_{ub} (10^{-3})$
2.0 – 2.6	$0.569 \pm 0.039 \pm 0.090$	$19.2 \pm 3.9 \pm 1.9$	$4.30 \pm 0.24 \begin{smallmatrix} +0.75 \\ -0.59 \end{smallmatrix} \pm 0.21$
2.1 – 2.6	$0.391 \pm 0.022 \pm 0.048$	$13.5 \pm 3.3 \pm 1.6$	$4.26 \pm 0.22 \begin{smallmatrix} +0.74 \\ -0.58 \end{smallmatrix} \pm 0.25$
2.2 – 2.6	$0.243 \pm 0.011 \pm 0.022$	$8.3 \pm 2.6 \pm 1.5$	$4.27 \pm 0.19 \begin{smallmatrix} +0.77 \\ -0.61 \end{smallmatrix} \pm 0.37$
2.3 – 2.6	$0.148 \pm 0.006 \pm 0.010$	$4.3 \pm 1.7 \pm 1.7$	$4.65 \pm 0.18 \begin{smallmatrix} +0.93 \\ -0.75 \end{smallmatrix} \pm 0.91$
2.4 – 2.6	$0.075 \pm 0.004 \pm 0.006$	$1.7 \pm 0.8 \begin{smallmatrix} +2.4 \\ -1.7 \end{smallmatrix}$	$5.28 \pm 0.27 \begin{smallmatrix} +1.29 \\ -1.00 \end{smallmatrix} \pm 3.76$

TABLE IX: The partial branching fraction $\Delta\mathcal{B}$, the predicted partial rate ζ for $B \rightarrow X_u e \nu$ decays and $|V_{ub}|$ for five electron momentum intervals, based on the SF parameters from the combined fit to *BABAR* moments ($\bar{\Lambda}^{SF} = (0.69 \pm 0.05) \text{ GeV}/c^2$, $\mu_\pi^{2SF} = (0.21 \pm 0.05) \text{ GeV}^2$) [27] based on BLNP calculations [24]. The errors are explained in the text.

Δp (GeV/c)	$\Delta\mathcal{B} (10^{-3})$	$\zeta(\Delta p)(\text{ps}^{-1})$	$ V_{ub} (10^{-3})$
2.0 – 2.6	$0.572 \pm 0.041 \pm 0.065$	$18.1 \pm 2.3 \pm 1.8$	$4.44 \pm 0.25 \begin{smallmatrix} +0.42 \\ -0.38 \end{smallmatrix} \pm 0.22$
2.1 – 2.6	$0.392 \pm 0.023 \pm 0.038$	$12.6 \pm 1.9 \pm 1.5$	$4.40 \pm 0.23 \begin{smallmatrix} +0.42 \\ -0.38 \end{smallmatrix} \pm 0.27$
2.2 – 2.6	$0.243 \pm 0.011 \pm 0.020$	$7.8 \pm 1.4 \pm 1.4$	$4.40 \pm 0.20 \begin{smallmatrix} +0.43 \\ -0.39 \end{smallmatrix} \pm 0.41$
2.3 – 2.6	$0.148 \pm 0.006 \pm 0.010$	$4.1 \pm 0.9 \pm 1.7$	$4.74 \pm 0.18 \begin{smallmatrix} +0.52 \\ -0.45 \end{smallmatrix} \pm 0.96$
2.4 – 2.6	$0.075 \pm 0.004 \pm 0.006$	$1.7 \pm 0.5 \begin{smallmatrix} +2.3 \\ -1.7 \end{smallmatrix}$	$5.29 \pm 0.27 \begin{smallmatrix} +0.74 \\ -0.59 \end{smallmatrix} \pm 3.66$

TABLE X: The total (\mathcal{B}) branching fraction for inclusive $B \rightarrow X_u e \nu$ decays for five electron momentum intervals. The spectral fractions f_u are based on calculations by Lange, Neubert and Paz [24] using SF parameters extracted from the combined fit [27] to all *BABAR* moments. The error definitions are the same as in Table III, and they are explained in the text above.

Δp (GeV/c)	$f_u(\Delta p)$	$\mathcal{B} (10^{-3})$
2.0 – 2.6	$0.252 \pm 0.018 \pm 0.019$	$2.27 \pm 0.26 \begin{smallmatrix} +0.33 \\ -0.28 \end{smallmatrix} \pm 0.17$
2.1 – 2.6	$0.176 \pm 0.017 \pm 0.019$	$2.22 \pm 0.23 \begin{smallmatrix} +0.32 \\ -0.27 \end{smallmatrix} \pm 0.24$
2.2 – 2.6	$0.109 \pm 0.014 \pm 0.020$	$2.22 \pm 0.20 \begin{smallmatrix} +0.33 \\ -0.28 \end{smallmatrix} \pm 0.40$
2.3 – 2.6	$0.057 \pm 0.009 \pm 0.023$	$2.58 \pm 0.20 \begin{smallmatrix} +0.47 \\ -0.36 \end{smallmatrix} \pm 1.04$
2.4 – 2.6	$0.023 \pm 0.005 \pm 0.033$	$3.21 \pm 0.33 \begin{smallmatrix} +0.80 & +4.47 \\ -0.58 & -3.21 \end{smallmatrix}$

for $\bar{\Lambda} = 0.69 \text{ GeV}/c^2$ and $\mu_\pi^2 = 0.21 \text{ GeV}^2$. Thus the uncertainty on the b -quark mass dominates. It should be noted that this dependence on $\bar{\Lambda}$ is a factor of two smaller for measurements based on the DN calculations.

These results are in excellent agreement with earlier measurements of the inclusive lepton spectrum at the $\Upsilon(4S)$ resonance, but their overall precision surpasses them [8–10, 12]. The earlier results were based on the DN calculations. We observe that for the same experimental input, i.e. the same measured lepton and photon spectra, the extracted values of $|V_{ub}|$ based on DN calculations agree very well with those based on BLNP calculations for the various momentum ranges under study, even though the corresponding partial branching frac-

tions may differ by one standard deviation.

The results presented here are also comparable in precision to, and fully compatible with, inclusive measurements recently published by the *BABAR* [54, 55] and Belle [56] Collaborations, based on two-dimensional distributions of lepton energy, the momentum transfer squared and the hadronic mass, with SF parameters extracted from $B \rightarrow X_s \gamma$ and $B \rightarrow X_c \ell \nu$ decays.

VII. ACKNOWLEDGMENTS

We would like to thank the CLEO and Belle Collaborations for providing detailed information on the extraction of the shape function parameters from the photon spectrum in $b \rightarrow s \gamma$ transitions. We are also indebted to M. Neubert and his co-authors B. Lange, G. Paz, and S. Bosch for providing us with detailed information on their calculations. We are grateful for the extraordinary contributions of our PEP-II colleagues in achieving the excellent luminosity and machine conditions that have made this work possible. The success of this project also relies critically on the expertise and dedication of the computing organizations that support *BABAR*. The collaborating institutions wish to thank SLAC for its support and the kind hospitality extended to them. This work is supported by the US Department of Energy and National Science Foundation, the Natural Sciences and Engineering Research Council (Canada), Institute of High Energy Physics (China), the Commissariat à l’Energie Atomique and Institut National de Physique Nucléaire et de

Physique des Particules (France), the Bundesministerium für Bildung und Forschung and Deutsche Forschungsgemeinschaft (Germany), the Istituto Nazionale di Fisica Nucleare (Italy), the Foundation for Fundamental Research on Matter (The Netherlands), the Research Council of Norway, the Ministry of Science and Technology of

the Russian Federation, and the Particle Physics and Astronomy Research Council (United Kingdom). Individuals have received support from CONACyT (Mexico), the A. P. Sloan Foundation, the Research Corporation, and the Alexander von Humboldt Foundation.

-
- [1] BABAR Collaboration, B. Aubert *et al.*, Phys. Rev. Lett. **87**, 091801 (2001); Phys. Rev. D **66**, 032003 (2002); Phys. Rev. Lett. **89**, 201802 (2002).
- [2] Belle Collaboration, K. Abe *et al.*, Phys. Rev. Lett. **87**, 091802 (2001); Phys. Rev. D **66**, 032007 (2002); Phys. Rev. D **66**, 0771102 (2002).
- [3] M. Kobayashi and T. Maskawa, Prog. Theor. Phys. **49**, 652 (1973).
- [4] M. Shifman and M. Voloshin, Sov. J. Nucl. Phys. **41**, 120 (1985); J. Chay, H. Georgi, and B. Grinstein, Phys. Lett. B **247**, 399 (1990); I. I. Bigi and N. Uraltsev, Phys. Lett. B **280**, 271 (1992); A.V. Manohar and M. B. Wise, Phys. Rev. D **49**, 1310 (1994); B. Blok, L. Koyrakh, M. A. Shifman and V. I. Vainshtein, Phys. Rev. D **49**, 3356 (1994).
- [5] M. Neubert, Phys. Rev. D **49**, 3392 (1994); C. W. Bauer and V. A. Manohar, Phys. Rev. D **70**, 034024 (2004).
- [6] I. I. Bigi, M.A. Shifman, N.G. Uraltsev, and V.I. Vainshtein, Int. J. Mod. Phys. A **9**, 2467 (1992).
- [7] M. Neubert, Phys. Rev. D **49**, 4623 (1994).
- [8] ARGUS Collaboration, H. Albrecht *et al.*, Phys. Lett. B **234**, 409 (1990); Phys. Lett. B **255**, 297 (1991).
- [9] CLEO Collaboration, R. Fulton *et al.*, Phys. Rev. Lett. **64**, 16 (1990); J. Bartelt *et al.*, Phys. Rev. Lett. **71**, 4111 (1993).
- [10] CLEO Collaboration, A. Bornheim *et al.*, Phys. Rev. Lett. **88**, 231803 (2002).
- [11] BABAR Collaboration, B. Aubert *et al.*, *Measurement of the Inclusive Electron Spectrum in Charmless Semileptonic B Decays*, Contributions to ICHEP02, Amsterdam (2002), hep-ex/0207081; BABAR Collaboration, B. Aubert *et al.*, *Determination of the Partial Branching Fraction for $B \rightarrow X_u \ell \nu$ and of $|V_{ub}|$ from the Inclusive Electron Spectrum near the Kinematic Endpoint*, Contribution to ICHEP04, Beijing (2004), hep-ex/0408075.
- [12] Belle Collaboration, A. Limosani *et al.*, *Measurement of $|V_{ub}|$ near the Endpoint of the Electron Momentum Spectrum from Semileptonic B-Meson Decays*, submitted to Phys. Lett., hep-ex/0504046 (2005).
- [13] L3 Collaboration, M. Acciarri *et al.*, Phys. Lett. B **436**, 174 (1998).
- [14] ALEPH Collaboration, R. Barate *et al.*, Eur. Phys. J. C **6**, 555 (1999).
- [15] DELPHI Collaboration, P. Abreu *et al.*, Phys. Lett. B **478**, 14 (2000).
- [16] OPAL Collaboration, R. Barate *et al.*, Eur. Phys. J. C **21**, 399 (2001).
- [17] F. DeFazio, and M. Neubert, JHEP **9906**, 017 (1999).
- [18] A. L. Kagan and M. Neubert, Eur. Phys. J. C **7**, 5 (1999).
- [19] S. W. Bosch, B. O. Lange, M. Neubert, and G. Paz, Nucl. Phys. B **699**, 335 (2004).
- [20] M. Neubert, Eur. Phys. J. C **40**, 165 (2005).
- [21] S. W. Bosch, M. Neubert and G. Paz, JHEP 0411, 073 (2004)
- [22] M. Neubert, *Impact of Four-Quark Shape Functions on Inclusive B Decay Spectra*, hep-ph/0411027 (2004).
- [23] M. Neubert, Phys. Lett. **B612**, 13 (2005) and private communication.
- [24] B. Lange, M. Neubert, and G. Paz, *Theory of Charmless Inclusive B Decays and the Extraction of $|V_{ub}|$* . hep-ph/0504071 (2005).
- [25] BABAR Collaboration, B. Aubert *et al.*, *Measurement of the $B \rightarrow X_s \gamma$ Branching Fraction and Photon Spectrum from a Sum of Exclusive Final States*, submitted to PRD, hep-ex/0508004 (2005).
- [26] BABAR Collaboration, B. Aubert *et al.*, Phys. Rev. Lett. **93**, 011803 (2004).
- [27] O. Buchmüller, H. Flächer, *Fits to Moment Measurements from $B \rightarrow X_c \ell \nu$ and $B \rightarrow X_s \gamma$ Decays Using Heavy Quark Expansions in the Kinetic Scheme*, hep-ph/0507253 (2005).
- [28] BABAR Collaboration, B. Aubert *et al.*, Nucl. Instr. Methods Phys. Res., Sect. A **479**, 1 (2002).
- [29] BABAR Collaboration, B. Aubert *et al.*, Phys. Rev. D **67** 031101 (2003).
- [30] GEANT4 Collaboration, S. Agostinelli *et al.*, Nucl. Instr. Methods Phys. Res., Sect. A **506**, 250 (2003).
- [31] E. Richter-Was, Phys. Lett. B **303**, 163 (1993).
- [32] Particle Data Group, K. Hagiwara, Phys. Rev. D **66**, 010001 (2002).
- [33] T. Sjöstrand, Comput. Phys. Commun. **82**, 74 (1994).
- [34] N. Isgur, D. Scora, B. Grinstein, and M. B. Wise, Phys. Rev. D **39**, 799 (1989); D. Scora, N. Isgur, Phys. Rev. D **52**, 2783 (1995).
- [35] I. I. Bigi, M. Shifman, and N. G. Uraltsev, Annu. Rev. Nucl. Part. Sci. **47**, 591 (1997).
- [36] I. Caprini, L. Lellouch, M. Neubert, Nucl. Phys. B **530**, 153 (1998).
- [37] B. Grinstein and Z. Ligeti, Phys. Lett. B **526**, 345 (2002).
- [38] CLEO Collaboration, J. Bartelt *et al.*, Phys. Rev. Lett. **82**, 3746 (1999).
- [39] Belle Collaboration, K. Abe *et al.*, Phys. Lett. B **526**, 258 (2002).
- [40] BABAR Collaboration, B. Aubert *et al.*, *Measurement of the $B \rightarrow D^*$ Form Factors in the Semileptonic Decay $\bar{B} \rightarrow D^{*+} e^- \bar{\nu}$* , Contribution to ICHEP04, Beijing (2004), hep-ex/0409047.
- [41] J. L. Goity and W. Roberts, Phys. Rev. D **51**, 3459 (1995).
- [42] G. C. Fox and S. Wolfram, Phys. Rev. Lett. **41**, 1581 (1978).
- [43] BABAR Collaboration, B. Aubert *et al.*, Phys. Rev. D **69**, 111104 (2004).
- [44] CLEO Collaboration, J. Bartelt *et al.*, Phys. Rev. Lett. **82**, 3746 (1996).
- [45] L. Gibbons, *The Status of $|V_{ub}|$* , Proceedings of the 9th

- International Conference on B Physics at Hadron Machines Pittsburgh, PA, AIP Conf. Proc. **722**, 156 (2004), hep-ex/0402009, and private communication.
- [46] N. Uraltsev, Int. J. Mod. Phys. A **14**, 4641 (1999), and private communication (2004).
- [47] A. H. Hoang, Z. Ligeti, and A. V. Manohar, Phys. Rev. D **59**, 074017 (1999).
- [48] T. van Ritbergen, Phys. Lett. B **454**, 353 (1999)
- [49] Particle Data Group, S. Eidelman et al., Phys. Lett. B **592**, 1 (2004).
- [50] M. Neubert, private communication (2004).
- [51] CLEO Collaboration, S. Chen *et al.*, Phys. Rev. Lett. **87**, 251807 (2001).
- [52] Belle Collaboration, P. Koppenburg *et al.*, Phys. Rev. Lett. **93**, 061803 (2004).
- [53] D. Benson, I. I. Bigi, and N. Uraltsev, Nucl. Phys. **710**, 371 (2005).
- [54] BABAR Collaboration, B. Aubert *et al.*, *Determination of $|V_{ub}|$ from Measurement of the Electron and Neutrino Momenta in Inclusive Semileptonic B Decays*, hep-ex/0506036, to be published in Phys. Rev. Lett. (2005).
- [55] BABAR Collaboration, B. Aubert *et al.*, *Measurement of the Partial Branching Fraction for Inclusive Charmless Semileptonic B Decays and the Extraction of $|V_{ub}|$* , hep-ex/0507017, Contribution to the Int. Symposium of Lepton-Photon Interactions, Uppsala (2005).
- [56] Belle Collaboration, H. Kakuno *et al.*, Phys. Rev. Lett. **92**, 101801 (2004).